ISBN 82-553-0573-4 No 3, March 1985
Applied Mathematics

# A NUMERICAL SOLUTION OF THE SECOND-ORDER, TWO-DIMENSIONAL WAVE DIFFRACTION PROBLEM FOR A SUBMERGED CYLINDER OF ARBITRARY SHAPE

by

TORGEIR VADA

ABSTRACT

The first- and second-order wave diffraction problems are solved for a submerged cylinder of arbitrary shape by the integral equation method based on Green's theorem. The integral equation is solved by an element method using cubic splines. The first- and second-order force, transmission and reflection coefficients are presented for two different contours. The results for the circular contour are compared with experimental results.

CONTENTS

# 1. INTRODUCTION

Two-dimensional, linear radiation and diffraction problems for submerged or semi-submerged bodies have been studied by many authors, and by a great variety of numerical methods. Several remarkable results have been found. One of the most interesting is the fact that the reflection coefficient of a submerged, restrained, circular cylinder is zero. This was first discovered by Dean [6] in 1948 and has been confirmed by all later studies of the same problem.

While the radiation problem has been solved for contours of many different shapes, most of the works on the diffraction problem have been confined to a circular contour. When other contours have been studied the additional assumption that the body is deeply submerged are made.

In a study of a circular cylinder which was restrained in the vertical direction, Longuet-Higgins [13] measured the mean horizontal force on the cylinder. He found that in many cases the force differed significantly from the result predicted by linear theory. He showed that this could be explained by non-linear effects.

An extensive experimental study of the restrained, circular cylinder has been made by Chaplin [4] and [5]. He has studied the flow field and pressure distribution around the cylinder and has measured the force components on the cylinder. This work also shows that non-linear effects can be important.

Fully non-linear solution methods in the time-domain have been developed by (among others) Vinje et al. [22]. The steady-state problem, however, must be studied by a perturbation method.

This has been done in the radiation problem for a semi-submerged body by several authors (for instance Potash [19]), but the second-order diffraction problem seems to be quite unexploited.

On this background we wanted to solve numerically the second-order diffraction problem for a submerged cylinder of arbitrary shape. We have done this by applying an integral equation method based on Green's theorem, where the equation is solved by using cubic splines. The integral equation method is chosen because it can be easily applied for contours of arbitrary shape. The cubics have been used because of their superior convergence properties compared to the more common choice of constant or linear polynomials. By this method we have been able to compute the second-order force and the second-order reflection and transmission coefficients. The results for two different contours are shown, and they clearly show that second-order effects can be important. A comparison with Chaplin's experiments shows a reasonable agreement.

## 2. FORMULATION OF THE PROBLEM

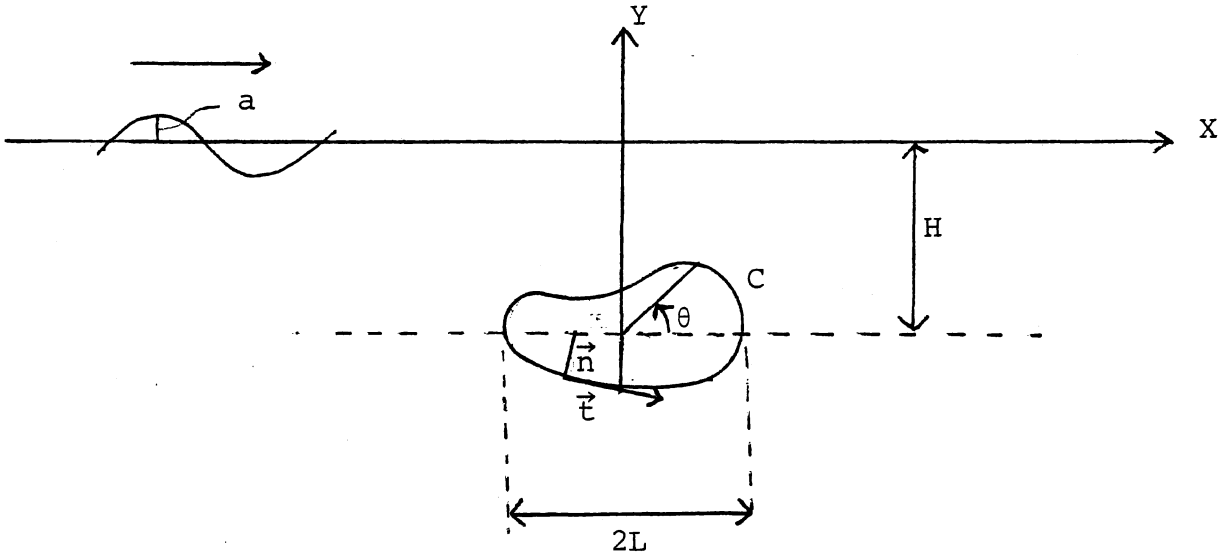


Fig. 2.1.

A 2-dimensional periodic wave with amplitude $a$ and frequency $\omega$ is scattered by a submerged cylinder with contour $C$ and its axis parallell to the wave crests. The fluid is assumed to be inviscid and incompressible and the motion is assumed to be irrotational. A velocity potential $\hat{\Phi}(X,Y,t)$ satisfying the Laplace equation then exists.

The kinematic and dynamic boundary conditions on the free surface are

$$\hat{\eta}_t(X,t) + \hat{\Phi}_x(X,\hat{\eta},t)\hat{\eta}_x(X,t) = \hat{\Phi}_y(X,\hat{\eta},t)$$

$$-g\hat{\eta}(X,t) = \hat{\Phi}_t(X,\hat{\eta},t) + \frac{1}{2}(\nabla\hat{\Phi}(X,\hat{\eta},t))^2 \qquad (2\text{-}1)$$

Elimination of the surface elevation gives the condition for $Y = \hat{\eta}$

$$\hat{\Phi}_{tt} + g\hat{\Phi}_y = -(2\hat{\Phi}_x\hat{\Phi}_{xt}+2\hat{\Phi}_y\hat{\Phi}_{yt}+\hat{\Phi}_x^2\hat{\Phi}_{xx}+\hat{\Phi}_y^2\hat{\Phi}_{yy}+2\hat{\Phi}_x\hat{\Phi}_y\hat{\Phi}_{xy}) \qquad (2\text{-}2)$$

We also assume that the cylinder is restrained and that the depth is infinite. This gives the additional conditions

$$\begin{cases} \hat{\Phi} = 0, & Y = -\infty \\ \hat{\Phi}_n = 0, & (X,Y) \in C \end{cases} \tag{2-3}$$

We now introduce the dimensionless quantities

$$\begin{cases} x = \frac{X}{L}, \quad y = \frac{Y}{L}, \quad \varepsilon = \frac{a}{L}, \quad h = \frac{H}{L}, \quad K = \frac{L\omega^2}{g}, \quad \tau = \omega t, \\ \eta(x,\tau) = \frac{1}{L}\hat{\eta}(X,t), \quad \Phi(x,y,\tau) = \frac{1}{\omega L^2}\hat{\Phi}(X,Y,t), \\ p(x,y,\tau) = \frac{1}{\rho g L}\hat{p}(X,Y,t), \quad \vec{F}(\tau) = \frac{1}{\rho g L^2}\hat{\vec{F}}(\tau), \\ M(\tau) = \frac{1}{\rho g L^3}\hat{M}(t) \end{cases} \tag{2-4}$$

where $\hat{M}$ is the moment with respect to the point $X = 0$, $Y = -H$ and $\hat{\vec{F}}$ is the force per unit length of the cylinder.

We shall neglect viscous effects and we therefore must assume that $\varepsilon$ is small. We then expand the potential $\Phi$ in a series

$$\Phi = \sum_{n=1}^{\infty} \varepsilon^n \Phi(n) \tag{2-5}$$

Since the motion is periodic we may write

$$\Phi^{(1)} = \mathrm{Re}\{\phi_0(x,y) + \phi_7(x,y)e^{-j\tau}\} \tag{2-6}$$

$$\Phi^{(2)} = \mathrm{Re}\{\phi_{20}(x,y) + \phi_{22}(x,y)e^{-2j\tau}\} \tag{2-7}$$

where $j$ is the imaginary unit and

$$\phi_0(x,y) = -\frac{1}{K} e^{Ky} e^{jKx} \tag{2-8}$$

is the potential of the incoming wave. Since the depth is infinite this potential is correct to third-order in $\varepsilon$. $\phi_7$, $\phi_{20}$ and $\phi_{22}$ are scattering potentials due to the presence of the cylinder.

It follows from the Bernoulli equation that the time-independent part of the second-order potential will only give a third-order contribution to the pressure and hence to the forces on the cylinder. In addition we believe that this potential must be found by methods very different from the present. We therefore neglect the potential $\phi_{20}$.

The boundary conditions for $\phi_7$ and $\phi_{22}$ are obtained by the introduction of (4) into (2) and (3) and Taylor expansion around $y = 0$. This gives

$$\begin{cases} (\phi_7)_n = -(\phi_0)_n \ , & (x,y) \in C & (2\text{-}9a) \\ (\phi_7)_y - K\phi_7 = 0 \ , & y = 0 & (2\text{-}9b) \\ (\phi_7)_y = 0 \ , & y = -\infty & (2\text{-}9c) \end{cases}$$

$$\begin{cases} (\phi_{22})_n = 0 \ , & (x,y) \in C & (2\text{-}10a) \\ (\phi_{22})_y - 4K\phi_{22} = f(x) \ , & y = 0 & (2\text{-}10b) \\ (\phi_{22})_y = 0 \ , & y = -\infty & (2\text{-}10c) \end{cases}$$

where

$$f(x) = \frac{Kj}{2}[3K^2(\phi^{(1)})^2 + \phi_{xx}^{(1)}\phi^{(1)} + 2(\phi_x^{(1)})^2]_{y=0} \qquad (2\text{-}11)$$

and

$$\phi^{(1)} = \phi_0 + \phi_7 \qquad (2\text{-}12)$$

In addition $\phi_7$ and $\phi_{22}$ must satisfy the Laplace equation and radiation conditions at $x = \pm\infty$. The radiation condition for $\phi_7$ is

$$(\phi_7)_x \mp jK\phi_7 = 0, \quad x = \pm\infty \qquad (2\text{-}13)$$

stating that the potential should be an outgoing wave at infinity. This may also be expressed as

$$\begin{cases} \phi_7(x,y) \to \dfrac{1-T_1}{K}\, e^{Ky} e^{jKx}, & x \to \infty \\ \phi_7(x,y) \to \dfrac{R_1}{K}\, e^{Ky} e^{-jKx}, & x \to -\infty \end{cases} \tag{2-14}$$

where $T_1$ and $R_1$ are the first-order transmission and reflection coefficients. When (14) is introduced into (11) we obtain

$$\lim_{x\to\infty} f(x) = 0 , \quad \lim_{x\to-\infty} f(x) = -4KjR_1 \tag{2-15}$$

Together with (10b) this indicates that $\phi_{22}$ may be written as

$$\phi_{22} = \phi_W + \phi_R$$

where $\phi_W$ at infinity represents a free outgoing wave with frequency $2\omega$ and wave number $4K$, i.e.:

$$(\phi_W)_x \mp 4jK\phi_W = 0 , \quad x = \pm\infty$$

and the remaining part $\phi_R$ is a potential satisfying

$$\phi_R = 0 , \quad x = \infty$$

$$\phi_R = +jR_1 , \quad x = -\infty$$

This gives the following "radiation" conditions for $\phi_{22}$

$$(\phi_{22})_x - 4jK\phi_{22} = 0 , \quad x = \infty \tag{2-16}$$

$$(\phi_{22})_x + 4jK\phi_{22} = -4KR_1 , \quad x = -\infty \tag{2-17}$$

The dynamic pressure is found from the Bernoulli equation, which takes the form

$$p(x,y,\tau) = -K(\Phi_\tau + \tfrac{1}{2}(\nabla\Phi)^2) \tag{2-18}$$

when the dimensionless quantities in (4) are introduced. We expand the pressure in a power series

$$p(x,y,\tau) = \sum_1^\infty \varepsilon^n p^{(n)}(x,y,\tau)$$

where we have

$$p^{(1)}(x,y,\ ) = \mathrm{Re}\{p_1(x,y)e^{-j\ }\}$$
$$p^{(2)}x,y,\tau) = \mathrm{Re}\{p_{20}(x,y) + p_{22}(x,y)e^{-2j\tau}\}$$

From (18) we then obtain

$$p_1(x,y) = Kj\phi^{(1)} \tag{2-19}$$

$$p_{20}(x,y) = -\frac{1}{4}K\phi_s^{(1)}\overline{\phi_s^{(1)}} \tag{2-20}$$

$$p_{22}(x,y) = 2Kj\phi_{22} - \frac{1}{4}K(\phi_s^{(1)})^2 \tag{2-21}$$

where the bar denotes the complex conjugate. The pressure force and moment is expanded in the same way:

$$\vec{F} = \mathrm{Re}\{\varepsilon\vec{F}_1 e^{-j\tau} + \varepsilon^2(\vec{F}_{20}+\vec{F}_{22}e^{-2j\tau})\} + O(\varepsilon^3) \tag{2-22}$$

$$M = \mathrm{Re}\{\varepsilon M_1 e^{-j\tau} + \varepsilon^2(M_{20}+M_{22}e^{-2j\tau})\} + O(\varepsilon^3) \tag{2-23}$$

where the components can be found by integration of the corresponding pressure component around the contour.

The surface elevation can be found from the dynamic boundary condition (1). Again we take

$$\varepsilon\eta(x,\tau) = \mathrm{Re}\{\varepsilon\eta_1(x)e^{-j\tau} + \varepsilon^2(\eta_{20}(x)+\eta_{22}e^{-2j\tau})\} + O(\varepsilon^3)$$

and then obtain

$$\eta_1(x) = Kj\phi^{(1)}(x,0) \tag{2-24}$$

$$\eta_{20}(x) = \frac{K}{4}(K^2\phi^{(1)}\overline{\phi^{(1)}} - \phi_x^{(1)}\overline{\phi_x^{(1)}})\Big|_{y=0} \tag{2-25}$$

$$\eta_{22}(x) = K(2j\phi_{22} - \frac{3}{4}K^2(\phi^{(1)})^2 - \frac{1}{4}(\phi_x^{(1)})^2)\Big|_{y=0} \tag{2-26}$$

For the component $\eta_{22}$ we have

$$\eta_{22}(x) = T_2e^{j4Kx} - \frac{1}{2}KT_1^2e^{j2Kx}, \qquad x \to \infty \tag{2-27}$$

$$\eta_{22}(x) = R_2e^{-j4Kx} - \frac{K}{2}e^{j2Kx} - \frac{R_1^2}{2}Ke^{-j2Kx}, \quad x \to -\infty \tag{2-28}$$

We notice that the cross-coupling terms between $\phi_0$ and $\phi_7$ exactly cancel the constant term in $\phi_{22}$ and hence for $x = -\infty$ the time-dependent part of $\eta$ consists of one incoming and one outgoing second-order Stokes-wave with frequency $\omega$ and a free outgoing wave with frequency $2\omega$. We define the second-order transmission and reflection coefficients $T_2$ and $R_2$ as the (normalized) amplitude of the free wave.

Our aim is now to compute the force, moment, reflection and transmission coefficients.

## 3. A REVIEW OF NUMERICAL METHODS AND PREVIOUS RESULTS

### i) Conformal mapping techniques

This method has been used by Dean [6] and Mehlum [14]. Dean used the transformation

$$\frac{z}{d} = \frac{-i(1-\zeta)}{1+\zeta} \quad , \quad \zeta = re^{i\theta} \quad , \quad d = \sqrt{h^2-1} \quad , \quad s = h-d$$

which maps the free surface, $y = 0$, on the circle $r = 1$ and the cylinder contour on the circle $r = s$. He then expands the potential in a modified Laurent-series where all the terms satisfy the boundary condition on $r = 1$ (i.e. the free surface condition). The boundary condition on $r = s$ together with an additional condition stating that the circulation is zero then provides a set of linear equations from which the coefficients can be found.

With this method Dean was able to show that the reflection coefficient of the circular cylinder was exactly zero. But the method is difficult to use if a complete solution of the diffraction problem is wanted, because the resulting linear equations are rather ill-conditioned.

Mehlum used a very similar method. The transformation

$$\frac{z}{d} = \frac{is+\zeta}{i\zeta+s} \quad , \quad \zeta = re^{i\theta} \quad , \quad d = \sqrt{h^2-1} \quad , \quad s = h-d$$

maps the cylinder on the circle $r = 1$ and the free surface on the circle $r = s$. He then expands the potential in a Laurent-series which automatically satisfies the boundary condition on $r = 1$ (i.e. the condition on the cylinder). From the condition on $r = s$ (the free surface condition) a recursion formula for the coefficients is obtained. When the incoming wave is specified this gives, after some mathematical manipulation, an analytical solution of the problem.

ii) The multipole method

The wave-source potential is a potential of the form

$$G(z,z_0;\gamma) = \ln(z-z_0) + h(z,z_0;\gamma) \tag{3-1}$$

where $h$ is a harmonic function chosen in such a way that

$$\begin{cases} G_y - \gamma G = 0 , & y = 0 \\ G_y = 0 , & y = -\infty \\ G_x \mp j\gamma G = 0 , & x = \pm\infty \\ G(z,z_0) = G(z_0,z) \end{cases} \tag{3-2}$$

In the multipole method the scattering potential is expanded in a series around the centre of the cylinder where all the terms are derivatives of (1) (with $z_0 = -ih$). From (2), (2-9b), (2-9c) and (2-13) we see that with $\gamma = K$ all the boundary conditions except the one on the cylinder will then be automatically satisfied. From this last condition the coefficients of the series are found. The method may, of course, be used in the radiation problems as well, with (2.9a) substituted by the appropriate condition.

Ursell [21], in 1950, used this method in a paper where he solved the linear diffraction problem for the circular cylinder. This paper confirmed Dean's result for the reflection coefficient and also provided an efficient solution method for the complete problem.

Ursell's work was extended by Ogilvie [18] . In addition to the diffraction problem he also solved the radiation problems and the problem with a free, neutrally buoyant cylinder. He also computed the mean force, $\vec{F}_{20}$ since this force component is given from the first-order potential only by (2-20). He discovered some

interesting results which we mention here although then are not directly related to our work:

1. The mean force on a circular cylinder oscillating along a straight line is directed vertically no matter how the line is oriented.
2. If the centre of the cylinder is moving in a circular orbit waves are generated in one direction only.
3. The reflection coefficient of the free cylinder is zero.

The second of these results has been the basis of an interesting wave-power project known as the Bristol cylinder. Reversing the time the result shows that a circular cylinder moving in a circular orbit should be able to absorb all the energy of a wave if the motion is properly tuned. This work has been carried out by Evans et al. and during the work many papers have been written where submerged cylinders are studied, see for instance [8].

iii) Integral equation methods

The methods previously described are very efficient when the cylinder is circular. If arbitrary contours are to be studied, however, integral equation methods are more convenient. These methods are, as the multipole method, based on the introduction of the wave-source potential or Green's function (1), and this function may be applied in two different ways.

One method is to write the potential we are seeking (for instance $\phi_7$) as a distribution of wave sources around the contour C:

$$\phi(z) = \oint_C \sigma(s)\,\mathrm{Re}\; G(z,\zeta(s);K)\,ds \qquad (3\text{-}3)$$

An integral equation for the source strength is obtained by taking the normal derivative of (3) and letting $z$ approach a point on the contour $z \to z(\hat{s})$. This gives

$$-\pi\sigma(\hat{s}) + \int_C \sigma(s)\,\mathrm{Re}\left\{\frac{\partial G(\zeta(s),z(\hat{s}))}{\partial n(\hat{s})}\right\} ds = \frac{\partial \phi(\hat{s})}{\partial n} \qquad (3\text{-}4)$$

From this equation $\sigma$ can be found when $\phi_n$ is known on the contour. The kernel in the integral is continuous, so the equation is an ordinary Fredholm equation of the second kind.

Grue & Palm [9] used a similar method, where they used vortices instead of sources in a study of the reflection coefficient for a deeply submerged, elliptic contour. Using this additional assumption they obtained an analytic expression for the reflection coefficient and showed that there were an infinite set of discrete wave-numbers for which the reflection coefficient was zero.

An alternative approach is to use Green's theorem:

$$\iint_\Omega (\alpha\nabla^2\beta - \beta\nabla^2\alpha)\,dA = \int_\sigma (\alpha\beta_n - \beta\alpha_n)\,ds \qquad (3\text{-}5)$$

where $\Omega$ is the fluid domain and $\sigma$ its boundary. If we put $\alpha = G(z,z_0;\gamma)$ and $\beta = \phi(z)$ we then have (for $z_0 \in \Omega$)

$$-2\pi\phi(z_0) = \int_\sigma (G\phi_n - \phi G_{n(s)})\,ds$$

If, in addition, we choose $\gamma = K$ the integral over the boundary will be zero except on the cylinder. This gives

$$-2\pi\phi(z_0) = \oint_C \left[G(z(s),z_0;K)\frac{\partial\phi(s)}{\partial n(s)} - \phi(s)\frac{\partial G(z(s),z_0;K)}{\partial n(s)}\right] ds \qquad (3\text{-}6)$$

i.e. $\phi$ is given by a distribution of both sources and dipoles around C. Finally, we let $z_0 \to z_0(\hat{s}) \in C$. This gives a Fredholm equation of the second kind for the potential $\phi$ when $\phi_n$ is known on C:

$$-\pi\phi(\hat{s}) + \int_C \phi(s)\frac{\partial G(s,\hat{s};K)}{\partial n(s)}ds = \int_C \frac{\partial \phi(s)}{\partial n(s)} G(s,\hat{s};K)ds \qquad (3\text{-}7)$$

We notice that the kernel of this equation is the conjugate of the kernel in (4). Hence either both or none of them have a unique solution. For the submerged cylinder it can be shown that the equations have a unique solution for all values of K (cfr. Grue & Palm [10]).

This method has been used in the study of the linear diffraction problem by several authors. Schnute [20] studied the transmission and reflection coefficient for two circular cylinders. Levine [12] studied wave reflection from a circular cylinder with its axis not parallell to the wave crest. In this case the cylinder will reflect some of the wave.

Both these authors solve (7) by the Galerkin method, expanding $\phi(=\phi_7)$ in a Fourier series. This method is efficient in some cases, especially if the cylinder is circular, elliptical or of a related shape, and the waves are long. In this case the Fourier-series converges rapidly. In the general case, however, with an arbitrary contour and arbitrary wave-lengths the method will often be computationally inefficient because the coefficients of the matrix of the linear equation system will be double integrals around the contour.

Alternatively one may write $\phi$ as a piecewise polynomial and use collocation to find the coefficients. The most common is to write $\phi$ as a piecewise constant or a piecewise linear

function. This method has been extensively used in the solution of radiation problems for semi-submerged cylinders, and it is also the method which we have chosen to use in this work. However, since we have been sceptical to the convergence properties of the piecewise constant or piecewise linear function we have applied a polynomial of a higher degree. We want to obtain better accuracy for two reasons: The first-order solution is input to the solution of the second-order problem, and integrals including the potential have to be computed over a long interval on the free surface.

## 4. THE SOLUTION METHOD

### i) The first-order problem

In this work we will apply the integral equation method based on Green's theorem, described in (3-5)-(3-7). A solution of (3-2) is

$$G(z,\zeta;\gamma) = \mathrm{Re}\{\ln(z-\zeta)-\ln(z-\bar{\zeta}) + 2\int_0^\infty \frac{e^{-i\nu(z-\bar{\zeta})}}{\gamma-\nu}\,d\nu - 2\pi j e^{-iK(z-\bar{\zeta})}\} \tag{4-1}$$

(Wehausen & Laitone [23]).

In the problems with semi-submerged cylinders this Green's function will result in an integral equation with irregular frequencies. When the cylinder is submerged this is not the case and we can use it without modification. With $\gamma = K$ this gives the integral equation (3-7) in the form

$$-\pi\phi_7(\hat{s}) + \oint_C \phi_7(s)\frac{\partial G(s,\hat{s};K)}{\partial n(s)}ds = \oint_C -\frac{\partial \phi_0(s)}{\partial n(s)} G(s,\hat{s};K)ds \tag{4-2}$$

when the boundary condition (2-9a) is used.

The contour $C$ is described by the parametric equations (cfr. fig. 2-1)

$$x = x(\theta), \quad y = y(\theta), \quad \theta \in [0,2\pi] \tag{4-3}$$

The normal and tangential vectors are

$$\vec{n} = \frac{1}{A}(-y'\vec{i}+x'\vec{j}) \tag{4-4}$$

$$\vec{t} = \frac{1}{A}(x'\vec{i}+y'\vec{j}) \tag{4-5}$$

where

$$A(\theta) = \sqrt{(x')^2+(y')^2} \tag{4-6}$$

We also have

$$ds = A(\theta)d\theta$$

which brings (2) on the more convenient form

$$-\pi\phi_7(\hat{\theta}) + \int_0^{2\pi}\phi_7(\theta)\frac{\partial G(\theta,\hat{\theta};K)}{\partial n(\theta)}A(\theta)d\theta$$

$$= \int_0^{2\pi} -\frac{\partial\phi_0(\theta)}{\partial n(\theta)}\,G(\theta,\hat{\theta};K)A(\theta)d\theta \qquad (4\text{-}7)$$

It is this equation we want to solve.

We now divide the interval $[0,2\pi]$ into $N$ subintervals $[\theta_{i-1},\theta_i]$ by

$$0 = \theta_0<\theta_1<\theta_2\ldots<\theta_{N-1}<\theta_N = 2\pi$$

and write the solution, $\phi_7$, as

$$\phi_7(\theta) = \sum_{i=1}^{N} q_i B_i(\theta) \qquad (4\text{-}8)$$

on $C$. Here $B_i$ is the cubic spline which is nonzero on $[\theta_{i-2},\theta_{i+2}]$ (see appendix A) and we define

$$\theta_{i\pm N} = \theta_i \pm 2\pi \qquad (4\text{-}9)$$

$\phi_7$ will now be a piecewise cubic polynomial with two continuous derivatives on $C$, hence the velocity has one continuous derivative. Since it is unreasonable to impose a velocity which is smoother than the contour, we also assume that the parametric equations (3) have one continuous derivative.

If this condition is not satisfied a modification of the splines, taut-splines, should be used (see de Boor [7]). Alternatively polynomials of a lower degree can be used, as in Andersen & Wuzhou [2], but as we shall soon see, higher order polynomials have favourable convergence properties.

We now put (8) into (7) and require that the equation should be exactly satisfied at the points $\theta_i$, $i=1,\ldots,N$. This gives the $N$ equations

$$-\pi \sum_{k=1}^{N} q_k B_k(\theta_i) + \sum_{j+1}^{N} q_j \int_0^{2\pi} B_j(\theta) \frac{\partial G(\theta,\theta_i;K)}{\partial n(\theta)} A(\theta)d\theta$$
$$= \sum_{j=1}^{N} \int_{\theta_{j-1}}^{\theta_j} - \frac{\partial \phi_0(\theta)}{\partial n} G(\theta,\theta_i;K)A(\theta)d\theta$$

In the residu-term only $k=i-1,i,i+1$ will contribute since all the other splines are zero at $\theta=\theta_i$. Likewise only the interval $<\theta_{j-2},\theta_{j+2}>$ will contribute to the integral term since $B_j(\theta)$ is zero elsewhere. We therefore obtain the following set of linear equations:

$$-\pi(B_{i-1}(\theta_i)q_{i-1} + B_i(\theta_i)q_i + B_{i+1}(\theta_i)q_{i+1})$$
$$+ \sum_{j=1}^{N} A_{ij}q_j = \sum_{j=1}^{N} B_{ij}, \quad i=1,2,\ldots,N \tag{4-10}$$

where

$$A_{ij} = \int_{\theta_{j-2}}^{\theta_{j+2}} B_j(\theta) \frac{\partial G(\theta,\theta_i;K)}{\partial n(\theta)} A(\theta)d\theta$$

$$B_{ij} = \int_{\theta_{j-1}}^{\theta_j} - \frac{\partial \phi_0(\theta)}{\partial n(\theta)} G(\theta,\theta_i;K)A(\theta)d\theta$$

In the computation of $A_{ij}$ we use (9) and in the residu-term the condition of zero circulation is buildt in because this condition implies that

$$\phi_7(\theta+2\pi) = \phi_7(\theta)$$

and hence

$$q_{i\pm N} = q_i \tag{4-11}$$

The integrals are computed by the 3-point Gauss formula on each interval $<\theta_{j-1},\theta_j>$, a method which is both computationally efficient and sufficiently accurate.

In practice all the coefficients $A_{i1},A_{i2},\ldots,A_{iN},B_{i1},B_{i2},\ldots,B_{iN}$ are computed simultaneously, where each interval

$<\theta_{j-1},\theta_j>$ will contribute to four of the A-coefficients and to $B_{ij}$. This is done because it is vital to minimize the number of computations of the Green's function.

An important feature of the method is that all the elements of the matrix $A_{ij}$ is small since they are integrals over only 4 intervals. The system of linear equations (10) is therefore diagonal dominant and can be easily solved by straightforward Gaussian elimination.

When this system is solved $\phi_7$ is known on C from (8) and the first-order and mean forces and moment can be computed by pressure integration. From (2-19), (2-20), (2-22) and (2-23) we have

$$\vec{F}_1 = \int_0^{2\pi} Kj\phi^{(1)}(\theta)\vec{n}(\theta)A(\theta)d\theta$$

$$\vec{F}_{20} = \int_0^{2\pi} -\frac{1}{4}K\phi_s^{(1)}(\theta)\overline{\phi_s^{(1)}(\theta)}\vec{n}(\theta)A(\theta)d\theta$$

$$M_1 = \int_0^{2\pi} Kj\phi^{(1)}(\theta)\vec{r}(\theta)\times\vec{n}(\theta)A(\theta)d\theta$$

$$M_{20} = \int_0^{2\pi} -\frac{1}{4}K\phi_s^{(1)}(\theta)\overline{\phi_s^{(1)}}\,\vec{r}(\theta)\times\vec{n}(\theta)A(\theta)d\theta$$

where $\vec{r} = x\vec{i} + (y+h)\vec{j}$, $\phi^{(1)} = \phi_0 + \phi_7$ and $\vec{n}$, $A(\theta)$ and $\phi_0$ are given from (4), (6) and (2-8) respectively. The tangential derivative of $\phi_7$ is found by differentiation of (8) since we have

$$\frac{\partial\phi_7}{\partial s} = \frac{\partial\phi_7}{\partial\theta}\frac{d\theta}{ds} = \frac{1}{A}\frac{\partial\phi_7}{\partial\theta}$$

From (3-6) and (2-9a) we have

$$\phi_7(z) = \frac{1}{2\pi}\int_0^{2\pi}\left(\frac{\partial\phi_0(\theta)}{\partial n(\theta)}G(z,\zeta(\theta);K)+\phi_7(\theta)\frac{\partial G(z,\zeta(\theta);K)}{\partial n(\theta)}\right)A(\theta)d\theta \quad (4\text{-}12)$$

and hence we can find $\phi_7$ everywhere in the fluid. With $z=x$ we can find the surface elevation $\eta_1(x)$ from (2-24), and after differentiation of (12) with respect to $x$ we can find $(\phi_7)_x(x,0)$ and thereby $\eta_{20}(x)$ from (2-25).

ii) The second-order problem

An integral equation for $\phi_{22}$ is obtained in the same way as the equation for $\phi_7$. We use Green's theorem and the Green's function (1).

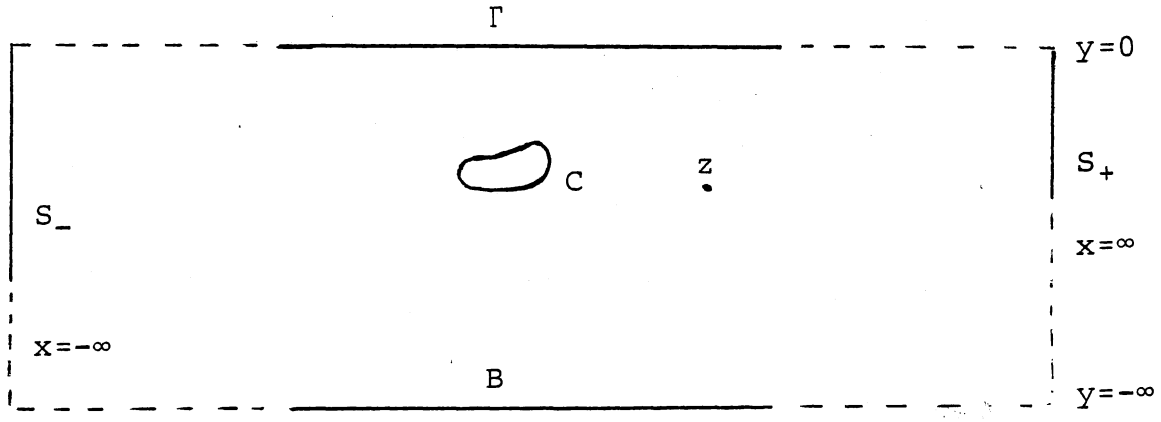


Fig. 4-1.

Green's theorem states that

$$-2\pi\phi_{22}(z) = \oint_{\Gamma+C+S_-+S_++B} \{\frac{\partial\phi_{22}(s)}{\partial n(s)}G(z,\zeta(s);\gamma)-\phi_{22}(s)\frac{\partial G(z,\zeta(s);\gamma)}{\partial n(s)}\}ds$$

From (2-10), (2-16), (2-17) and (3-2) we see that with $\gamma=4K$ the integrals over $B$ and $S_+$ vanish whereas the remaining contributions will be

$$-2\pi\phi_{22}(z) = \int_C -\phi_{22}(s)\frac{\partial G(z,\zeta(s);4K)}{\partial n(s)}ds + \int_\Gamma f(\xi)G(z,\xi;4K)d\xi + \int_{S_-} 4KR_1G(z,\zeta(s);4K)ds$$

where the function $f(\xi)$ is defined in (2-11). Using (12), $f(\xi)$ can be computed since this equation will give $\phi_7(x,0)$, $(\phi_7)_x(x,0)$ and $(\phi_7)_{xx}(x,0)$. The derivatives are computed by differentiation of (12) since this will avoid the loss of accuracy which would be present if numerical derivatives were used.

The free surface integral is truncated by setting

$$\int_\Gamma f(\xi)G(z,\xi;4K)d\xi \approx \int_{x_L}^{x_R} f(\xi)G(z,\xi;4K)d\xi$$

where $x_R$ is chosen so large that $f(\xi)$ is sufficiently small for all $\xi > x_R$, and $x_L(<0)$ must be so large in value that

$$f(\xi) \approx -4KjR_1 \qquad \forall \xi < x_L$$

$$G(z,\zeta;4K) \approx A(z)e^{-4jK\xi}e^{4K\eta} \qquad \forall \xi < x_L$$

We then have

$$\int_{S_-} 4KR_1 G(z,\zeta(s);4K)ds \approx 4KR_1 A(z)e^{-4jKx_L}\int_{-\infty}^{0} e^{4K\eta}d\eta$$

$$= R_1 A(z)e^{-4jKx_L}$$

$$= R_1 G(z,x_L;4K)$$

and the sum of the integrals over $S_-$ and $\Gamma$ will be independent of $x_L$.

Substituting the angle $\theta$ for $s$ we now have

$$-2\pi\phi_{22}(z) = \int_0^{2\pi} -\phi_{22}(\theta)\frac{\partial G(z,\zeta(\theta);4K)}{\partial n(\theta)} A(\theta)d\theta$$

$$+ \int_{x_L}^{x_R} f(\xi)G(z,\xi;4K)d\xi + R_1 G(z,x_L;4K). \qquad (4\text{-}13)$$

Letting $z \to x(\hat{\theta}) + iy(\hat{\theta})$ we then obtain the integral equation for $\phi_{22}$

$$-\pi\phi_{22}(\hat{\theta}) + \int_0^{2\pi} \phi_{22}(\theta)\frac{\partial G(\hat{\theta},\theta;4K)}{\partial n(\theta)} A(\theta)d\theta$$

$$= \int_{x_L}^{x_R} f(\xi)G(z(\hat{\theta}),\xi;4K)d\xi + R_1 G(z(\hat{\theta}),x_L;4K) \qquad (4\text{-}14)$$

This equation is solved in exactly the same way as the first-order equation, (7). We write

$$\phi_{22} = \sum_{i=1}^{N} \gamma_i B_i(\theta) \qquad (4\text{-}15)$$

where $\gamma_i$ are the solution of the linear equations

$$-\pi(B_{i-1}(\theta_i))\gamma_{i-1} + B_i(\theta_i)\gamma_i + B_{i+1}(\theta_i)\gamma_{i+1})$$
$$+ \sum_{j=1}^{N} C_{ij}\gamma_j = D_i \,, \quad i=1,2,\ldots,N \qquad (4\text{-}16)$$

where

$$C_{ij} = \int_{\theta_{j-2}}^{\theta_{j+2}} B_j(\theta)\frac{\partial G(\theta_i,\theta;4K)}{\partial n(\theta)} A(\theta)d\theta$$

$$D_i = \int_{x_L}^{x_R} f(\xi)G(z(\theta_i),\xi;4K)d\xi + R_1 G(z(\theta_i),x_L;4K)$$

and we also assume that the circulation is zero which gives

$$\phi_{22}(\theta+2\pi) = \phi_{22}(\theta)$$

and hence

$$\gamma_{i\pm N} = \gamma_i$$

When (16) is solved $\phi_{22}$ is known on C from (15) and the second-order oscillatory force and moment can be found by pressure integration. From (2-21)-(2-23) we have

$$\vec{F}_{22} = \int_0^{2\pi} [2Kj\phi_{22}(\theta) - \tfrac{1}{4}K(\phi_s^{(1)})^2]\vec{n}(\theta)A(\theta)d\theta \qquad (4\text{-}17)$$

$$M_{22} = \int_0^{2\pi} [2Kj\phi_{22}(\theta) - \tfrac{1}{4}K(\phi_s^{(1)})^2]\vec{r}(\theta)\times\vec{n}(\theta)A(\theta)d\theta \,,$$

$$\vec{r} = x\vec{i} + (y+h)\vec{j} \qquad (4\text{-}18)$$

From (13) $\phi_{22}$ can be found anywhere in the fluid when it is known on the contour. In particular $\phi_{22}(x,0)$ can be found and thereby $\eta_{22}(x)$ is found from (2-26).

iii) Convergence test

There are several ways in which the numerical results can be checked. In appendix B an alternative computation method for $\vec{F}_{22}$ and $M_{22}$ is described. The results from this method can be compared with the direct pressure integration described above. In addition all the equations (2-15) and (C-1)-(C-5) should be satisfied. We have been satisfied with the convergence when all these tests were satisfied with an error of 0.01 or less.

We have made these checks for the pontoon with $h = 1.0$, $K = 0.5$ and $h = 1.0$, $K = 2.5$ in order to find out the number of elements needed, how they should be distributed and what values we should use for $x_L$ and $x_R$.

For the long wave, $K = 0.5$, we found that 22 elements were needed on the contour and that they should be distributed almost equidistantly around the contour, with only a few extra elements on the upper part. We also found that we had to choose $x_L \approx -8$ and $x_R \approx 6$. This gave a total CPU-time of about 2.30 minutes.

In appendix B a méthod is described in which the second-order oscillatory force and moment are found from first-order potentials only. This might look as a tempting approach. However, instead of the $\phi_{22}$ - problem we have to solve three extra first-order problems and compute the potentials on the free surface from $x_L$ to $x_R$. It is vital to compute these potentials simul-

taneously in order to minimize the number of computations of the Green's function, but even when this is done the necessary computation time will be larger than with our method. This is due to the fact that about 60% of the total computation time is spent on the computation of the function $f(x)$, and when this is done the integral equation for $\phi_{22}$ can be solved just as fast as the first-order equations. And if the second-order motion is to be studied, as in this work, $\phi_{22}$ has to be computed anyway.

We also wanted to compare the convergence of our method, in which cubic elements is used, with the same method with linear elements distributed in the same way as the cubics. To do this we studied the first-order problem only, and the solution of this can be obtained with only 11 cubic elements and a CPU-time of about 5 seconds.

When linear elements are used it is consistent to use the midpoint rule in the computation of the integrals, and therefore the computation time for an integral over one interval is only one third of the time needed with the cubics. But it turned out that in order to obtain the same accuracy as the one obtained by the 11 cubics we had to use 130 linear elements, with a computation time of 6.30 minutes! This shows that the introduction of cubic elements improves the method considerably, and it seems almost like a necessity in the solution of the second-order problem.

For the shorter wave, $K = 2.5$, we also had to use 22 elements, but they were distributed in a different manner. In this case there is not much happening on the lower part of the cylinder (see for instance fig, 22-25 in the figure section). Because of this, the majority of the elements are on the upper

part. Some computation time was saved in comparison with the long wave however since $x_L = -5$, $x_R = 5$ turned out to be sufficient in this case. This gave a total CPU-time of 2.15 minutes.

The linear elements, on the other side, converged much faster in this case than for $K = 0.5$. But they still were more time-consuming than the cubics.

The computations have been done by a set of SIMULA/ALGOL-programs on a DEC-10 computer. We have tried to reduce the number of calculations of the Green's function, but apart from this no particular efforts have been made to optimize the programs. With more optimized FORTRAN programs on a better computer, for instance a CYBER, we therefore believe that the computation times mentioned above can be reduced by a factor of 5-10. An extreme improvement, however, can be obtained if an efficient computation method for the Green's function is at hand. We have noticed that the computation time tends to depend almost linearly on the number of computations of this function, so there seems to be little doubt about where most of the time is consumed.

## 5. THE FIRST-ORDER SOLUTION

We have applied the method described in this work to the two contours shown in fig. 1. They are both parts of a class of contours which are often called Lewis-forms. These contours are given by the equations

$$x(\theta) = \frac{\cos\theta - \alpha\cos 3\theta}{1-\alpha}$$
$$y(\theta) = b\,\frac{\sin\theta + \alpha\sin 3\theta}{1-\alpha}$$

where $\alpha = 0$, $b = 1$ gives the circle, and the other contour is given by $\alpha = 0.1$, $b = 0.5$. These parameters are chosen so that the contour is very similar to the pontoons of an Aker platform. (For this pontoon, $L = 7.2$ m).

### i) The first-order force and moment

The first-order force on the circle is shown in figs 3 and 4. The results agree completely with the results of Ogilvie [18] but they are presented in a different manner. We notice that the force increases significantly, but not dramatically for all wave numbers when $h$ is decreased. The wave-number for which the force has its maximum varies only very slightly with $h$.

We have also computed the force on the cylinder from the linear Morrison equation

$$F_i = (m_{ii}+m)\dot{U}_i \quad , \quad i=1,2$$

where $\dot{U}_i$ is taken as the horizontal ($i=1$) or vertical ($i=2$) acceleration of the undisturbed incoming wave in the point $x=0$, $y=-h$. $m_{ii}$ is the added mass in an infinite fluid and $m$ is the displaced water mass. In our non-dimensional units we then have

$$\dot{U}_x = \dot{U}_y = Ke^{-Kh}$$

which gives

$$F_x = F_y = 2\pi Ke^{-Kh} \qquad (5\text{-}1)$$

for the circle. The result is shown by the dotted lines in figs 3 and 4. We see, as expected, that Morrison's equation predicts a force maximum for shorter waves than our method for small values of $h$. (The maximum point is $K = \frac{1}{h}$ which depends strongly on $h$). For the largest value of $h$, however, the agreement is very good (fig. 4). Even more surprising is the fact that the maximum value is very well predicted for the other values of $h$ as well. Hence, if only this value is needed the Morrison equation is quite sufficient. However, if one is interested in the force for a given wave number or the phase, it will fail. In these cases the full analysis is needed.

Another approximative method which may be used to compute the force on the circle is the application of Milne-Thomson's circle therem ([16]). Using this theorem it is easy to modify the potential of the incoming wave in such a way that the boundary condition on the cylinder is satisfied. The resulting potential can be integrated analytically around the circle. This method is good when $Kh$ is large (see Ogilvie [18]). On the other hand, the Morrison equation is good when $KL$ is small (see Newman [17]). On this background it is quite surprising that the Milne-Thomson method gives exactly the same result as the Morrison formula. This explains why (1) seems to give good results for both very small and very large wave numbers.

The results for the pontoon is shown in figs 7 and 8. The h-values are chosen such that the distance from the free surface to the top of the cylinder is the same as in the circular case. The behaviour of the curves are quite similar to the curves for the circle with one interesting exception: There seems to be distinct wave numbers for which the force is zero and these points vary quite a lot with h. Hence, in the vicinity of such a point the force will increase when h increases. It is also interesting to notice that both the maximum points and the zero points are different for the two components. The increase of the vertical and decrease of the horizontal component in magnitude compared with the circle is as expected.

For the pontoon the Morrison equation gives

$$F_x = 2.946Ke^{-Kh}\ , \quad F_y = 5.554Ke^{-Kh}$$

and we notice the same phenomenon here as with the circle. The formula gives a very good estimation of the maximum values but not of the maximum points. For the prediction of the force for a given wave number the deviation from the "correct" value is much larger for the pontoon than it was for the circle, particularly for the larger wave numbers.

The moment is shown in fig. 11. As expected it has its maximum for wavelengths about twice the horizontal extension of the pontoon, but the maxima are much less distinct than they were for the force components.

ii) The free cylinder

To illustrate a consequence of the different variation with K of the force and moment we have computed the responce of a freely floating pontoon to an incoming wave. If $\xi_1, \xi_2$ and $\xi_6$ are the amplitudes of the sway, heave and roll motion respectively and $X_i$ are the components of the exciting force and moment we have in dimensionless units (cfr. Newman [15])

$$\sum_{j=1,2,6} \xi_j A_{ij} = \varepsilon X_i \ , \quad i=1,2,6$$

where

$$A_{ij} = -(M_{ij}+a_{ij}) - jb_{ij}$$

and $M_{ij}, a_{ij}$ and $b_{ij}$ are the body mass, added mass and damping. For the pontoon only $A_{11}, A_{16}, A_{66}$ and $A_{22}$ will be non-zero.

The added mass and damping are found by solving the radiation problems. This is done in exactly the same way as we solve the diffraction problem with $(-\phi_0)_n$ substituted by $n_x, n_y$ or $(\vec{r}\times\vec{n})\cdot\vec{k}$ ($\vec{r} = x\vec{i} + (y+h)\vec{j}$) in the integral equation (4-7). With $h = 1.0$ and $\varepsilon = 0.3$ we then obtain

$$\xi_1 = \begin{cases} 0.38 + 0.05j \ , & K=0.5 \\ \approx 0 \ , & K=2.5 \end{cases}$$

$$\xi_2 = \begin{cases} 0.10 - 0.50j \ , & K=0.5 \\ 0.04 - 0.05j \ , & K=2.5 \end{cases}$$

$$\xi_6 = \begin{cases} 0.13 + 0.02j \ , & K=0.5 \\ 0.16 + 0.03j \ , & K=2.5 \end{cases}$$

The resulting motion is illustrated in figs 16 and 17 where we see that for $K = 0.5$ the sway and heave dominates, with only a slight roll motion, whereas for $K = 2.5$ the sway and heave motion has become very small while the roll is still of the same size.

iii) The mean force and moment

The mean vertical force on the circle is shown in fig. 5. We see that it has its maximum for the same wave number as the first-order force but it decays more slowly with increasing K. On the other hand it is more sensitive to the value of h. We also notice that it is always positive. This result is also given by Ogilvie [18] and our results agree completely with his.

The mean horizontal force is related to the reflection coefficient throught (C-2) and hence it is zero for all K for the circle since the reflection coefficient is always zero.

The mean vertical force on the pontoon is shown in fig. 9. We notice the same features as with the circle, but we may also notice that compared to the first-order force the mean force is more important for the pontoon than it is for the circle.

The mean horizontal force is shown in fig. 10 (notice the difference in scales). The maximum values of the three curves correspond to reflection coefficients of 0.36, 0.23 and 0.16. We notice that there is no significant reflection of waves with wave number >2.

The mean moment is shown in fig. 15. As expected it is negative, i.e. it will give a rotation in the same direction as the fluid particles, but it is very small and must be regarded as quite uninteresting.

## 6. THE SECOND-ORDER SOLUTION

### i) Force and moment

The second-order oscillatory force on the circle is shown in fig. 6 where it is compared to the first-order force. We notice the following differences

- The maximum value of the second-order component increases much more dramatically with decreasing $h$
- The maximum value is reached for a smaller wave number
- The value decreases very rapidly when $K$ is larger than the maximum point and for $K>2$ the second-order force is almost zero.

The results for the pontoon is shown in fig. 12-14. Again we notice the same features as for the circle. In addition we have the following:

- The relative importance of the second-order force in comparison with the first-order force is larger for the horizontal component than it is for the vertical component
- The relative importance of the second-order force is larger for the pontoon than it is for the circle for the smallest value of $h$, but almost the same for the two others.
- The second-order force also has zero-points, just as the first-order components and the zeros are found for smaller values of $K$.

The first of these phenomena is somewhat surprising, whereas the second is not. The shape of the body will obviously be more important the closer the cylinder is to the free surface. This can also be seen by a comparison of the vertical first-order force on the two contours. The difference is smallest for the largest value of $h$.

Very interesting is the result for the moment shown in fig. 14. We see that the second-order moment shows a similar behaviour as the force does, even though the maximum point is more sensitive to the value of $h$. This is a contrast to the first-order quantities. The result of this is that, unless $\varepsilon$ is very small, the second-order term will give the dominant contribution to the moment for the long waves.

ii) The tangential velocity and pressure distribution on the cylinder

We have computed the tangential velocity and pressure distribution around the contour for a "long" wave ($K = 0.5$) and a "short" wave ($K = 2.5$).

The results for the short wave are shown in fig. 22-25 and 32. We notice that both the velocity and the (dynamic) pressure is almost zero on the lower half of the cylinder. We also see that the result for the circle and the pontoon are almost equal, except for the mean pressure (fig. 32). This last quantity seems to depend only on the distance from the point on the cylinder contour to the free surface. The second-order oscillatory quantities are not shown in this case since they are very small.

As expected the results for the long wave are more complicated. The first- and second-order oscillatory velocities are shown in fig. 18-21 for two different values of $h$. We point out the following features:

- The second-order velocity decays much faster with increasing $h$ than the first-order velocity does

- The second-order velocity is much larger on the pontoon than it is on the circle
- The second-order velocity is very small on the lower half of the cylinder
- On the pontoon the first-order velocity has local maxima/minima at the corners, while the second-order velocity varies more smoothly around the contour.

The oscillatory pressure components are shown in fig. 26-29. Again we see that the second-order quantity is very sensitive to the value of h, whereas the first-order is not. The first-order pressure is very similar on the circle and the pontoon, but the second-order pressure is much larger on the pontoon, where it also has a significant value on the lower parts. The figures illustrate clearly the increased importance of second-order effects on this contour.

The mean pressure in the long wave case is shown in fig. 30 and 31 where we notice very strong maxima at the corners of the pontoon.

In the figures the mean dynamic pressure is shown as a positive quantity. These figures actually show $-p_{20}$. The mean pressure is negative and results in a mean force which is directed upwards, as we have seen in the previous chapter.

iii) Reflection and transmission coefficients

The second-order transmission coefficient, defined in (2-27) is shown in fig. 33 (circle) and 34 (pontoon). We notice that this coefficient can be very large, but as the other second-order

quantities it is only significant for $K < 2.5$. In fig. 36 the free surface is shown in natural scale for one particular case. We clearly see that the transmitted wave is a superposition of one wave with wave number $K$ and one wave of comparable amplitude with wave number $4K$. At first sight this effect seems to violate the energy conservation law, but this is not the case. The 4K-wave will give a fourth-order contribution to the energy flux and this may be balanced by terms including quantities that we are not able to compute such as the stationary second-order potential and the third-order potentials.

The first- and second-order reflection coefficient for the pontoon is shown in fig. 35 (notice the difference in scale from fig. 33 and 34). Again we notice that the second-order contribution can be very significant, but the effect is not as dramatic as it were for the transmitted wave.

For the circle, $R_1 \equiv 0$, as we have mentioned several times. We were therefore particularly interested in finding out if the same was true for the second-order coefficient. In our computation we found values of $R_2$ of the order 0.01. The result seems to be significant, since we obtained a nice sinusoidal behaviour of the potential. Hence, we believe that there is a very small reflected second-order wave. For all practical purposes, however, we have $R_2 \approx 0$.

## 7. DISCUSSION AND COMPARISON WITH EXPERIMENTS

The diffraction problem with the circular cylinder has, as previously mentioned, been studied experimentally by Chaplin [5]. In his work the different force components have been measured. He found that viscous effects become important when the Keulegan-Carpenter number, which he defines as

$$Kc = \pi\varepsilon e^{-Kh} \tag{7-1}$$

is large. From his results we take the limit as $Kc=1$. For larger values of $Kc$ our theory will not be applicable. The vertical force on the cylinder can be written as

$$F_y = \sum_{n=0}^{\infty} f_n e^{-jn\tau}$$

Chaplin studies the first four components which may be written as

$$\begin{cases} f_0 = a_{02}Kc^2 + a_{04}Kc^4 + \ldots \\ f_1 = a_{11}Kc + a_{13}Kc^3 + \ldots \\ f_2 = a_{22}Kc^2 + a_{24}Kc^4 + \ldots \\ f_3 = a_{33}Kc^3 + \ldots \end{cases} \tag{7-2}$$

where the coefficients $a_{02}, a_{11}$ and $a_{22}$ are related to our force components $(F_{20})_y, (F_1)_y$ and $(F_{22})_y$ through (1) and (2-22). $a_{02}$ and $a_{11}$ agree completely with Ogilvie's results which we have reproduced as well. The comparison between $a_{22}$ and $F_{22}$ is shown in the following table:

| Parameters | Case | $a_{22}\pi^2 e^{-2Kh} = \lvert(F_{22})_y\rvert$ | |
|---|---|---|---|
| | | Theory | Experiment |
| h=2.0, K=0.206 | I | 0.31 | 0.39 |
| h=2.0, K=0.365 | II | 0.33 | 0.33 |
| h=2.0, K=0.570 | III | 0.21 | 0.21 |
| h=2.0, K=0.821 | IV | 0.09 | 0.16 |
| h=3.0, K=0.206 | V | 0.06 | 0.05 |
| h=3.0, K=0.365 | VI | 0.04 | 0.05 |

Hence, compared with the curve for $h = 2.0$ in fig. 16, the experimental results agree very well near the top of the curve, but they indicate that the maximum value is obtained for a smaller value of $K$ (case I) and that the force decreases more slowly when $K$ is increased beyond $K = 0.6$ than our theory predicts (case IV).

Of the other coefficients in (2) $a_{04}$ and $a_{24}$ are very small. The most significant higher-order contribution is the correction of the first harmonic, $a_{13}$. This coefficient is always negative and hence reduces the force. For wave amplitudes $\varepsilon > 0.3$ the term $a_{13}Kc^3$ will be of the same size as $a_{22}Kc^2$. The third harmonic ($f_3$) will be significant in case III but unless $Kc$ is almost one it will be smaller than the second-harmonic.

In fig. 37-42 the flow regimes for various wave numbers and wave amplitudes are illustrated. Above the upper full line the incoming wave breaks, since it has been shown that this will occure when the wave steepness, $\varepsilon K$, is greater than 0.4434. Above the dashed line Chaplin's experiments show that viscous effects will be important. The line is given by $Kc = 1.0$ for the circle. For the pontoon we assume that viscous effects will be more important and we have taken the limit as $Kc = 0.8$, which of course is only a crude estimate. It is only below these lines that our theory can be applied.

An important aspect of a second-order theory is that it gives an indication of the validity of linear theory. A possible criterion is

$$\varepsilon |(F_{22})|_x < 0.1 \; |(F_1)_x|$$
$$\varepsilon |(F_{22})|_y < 0.1 \; |(F_1)_y|$$

This is satisfied for parameters below the lower full line.

The dotted line indicates the breaking limit. For parameters above this line the wave breaks when it passes the cylinder. We notice that for the long waves this occurs for a much smaller value of the wave steepness than the breaking limit for the incoming Stokes-wave. The curves are obtained from purely visual experiments which we have performed in the wave-tank at our institute. This tank is 0.5×0.5×16.0 m and the cylinder radius was 10 cm. It is interesting to notice that the $e^{-2j\tau}$-component of the force can be calculated with reasonable accuracy even for points above this line, since we have previously mentioned that this force component is described by the coefficient $a_{22}$ in (2) for all $Kc < 1$. The most important higher-order effect is the reduction of the $e^{-j\tau}$-component.

There are no experimental data of the second-order transmission coefficient. Longuet-Higgins [13] has measured it for a cylinder which was restrained only in the vertical direction. In this case there is a reflected wave and hence it is reasonable to expect that the transmitted wave is somewhat smaller in this case than it will be when the cylinder is restrained. For $K = 0.3$, $h = 1.67$ he found $T_2 = 1.23$ whereas we obtained $T_2 = 1.85$. Visual comparisons between photographs taken in the wave-tank at our institute, and numerical results of the type shown in fig. 35 show good agreement. However, the total wave amplitude in the experiments is somewhat smaller than we obtain. This may be due to energy dissipation, but it is more likely that it is due to a third-order effect which reduces the amplitude of the first harmonic. We therefore expect that the results presented in fig. 33-35 give reasonably good values for the amplitude of the second harmonic.

ACKNOWLEDGEMENTS

This thesis has been written under surveillance of Prof. Enok Palm who has provided me with helpful advices at several stages of the work. I also want to thank John Grue who has been chosen as the victim at several times when I wanted a discussion and also provided me with photographs of the wave field.

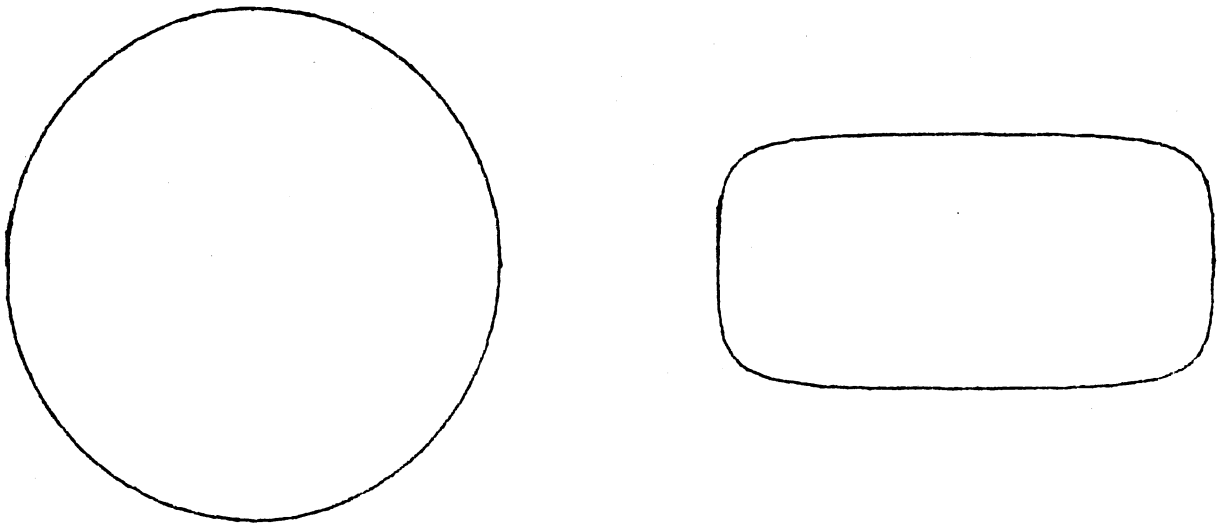

Fig. 1. The contours.

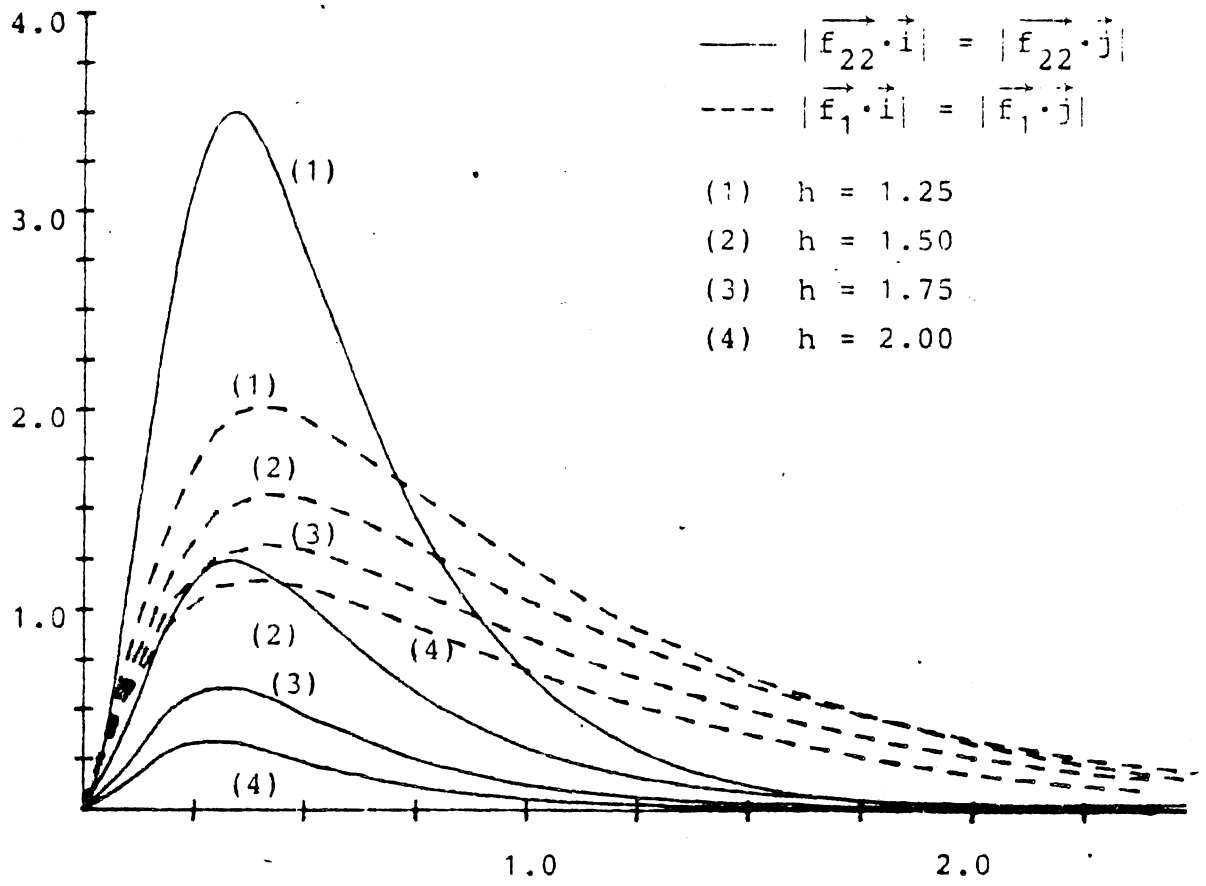


Fig. 2. Amplitude of first- and second-order oscillating forces on the circle. From this figure we have concluded that values of $h$ for which $h-b < 0.5$ cannot be handled by a perturbation method, except for short waves. Hence only results for cases with $h-b \geq 0.5$ are presented in the following figures.

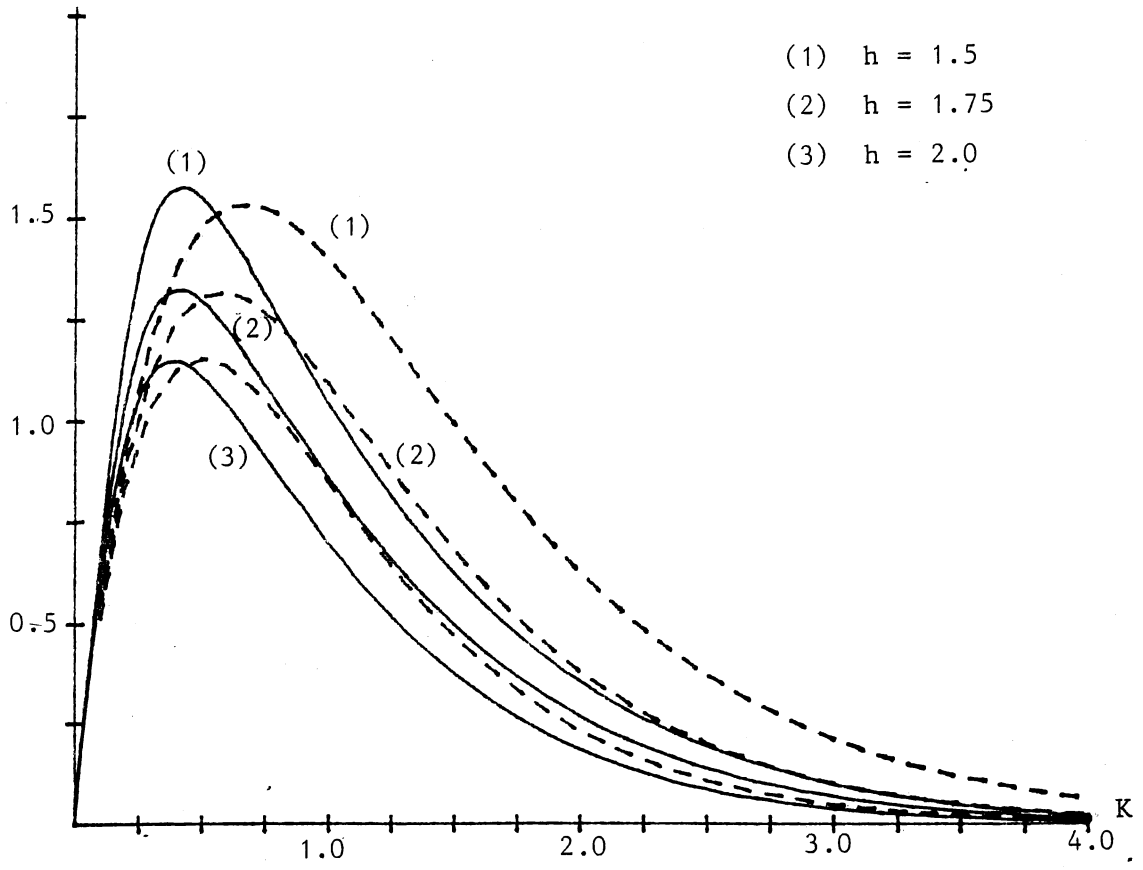


Fig. 3. First-order oscillatory force on the circle for h = 1.5, 1.75, 2.0. Dotted line: The result due to Morrison's formula.

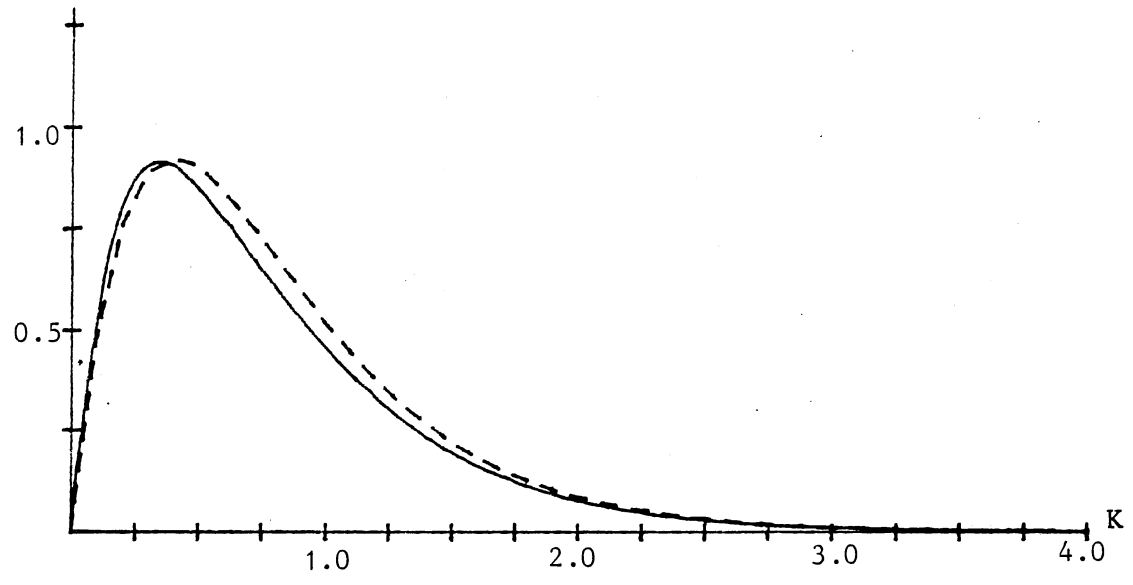


Fig. 4. As fig. 3, but with h = 2.5.

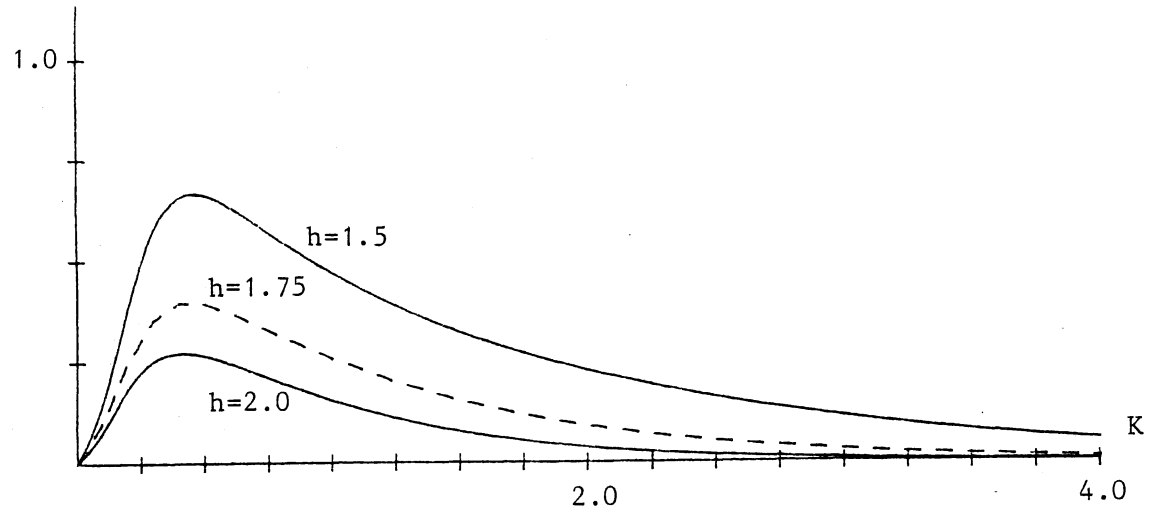


Fig. 5. The mean vertical force on the circle.

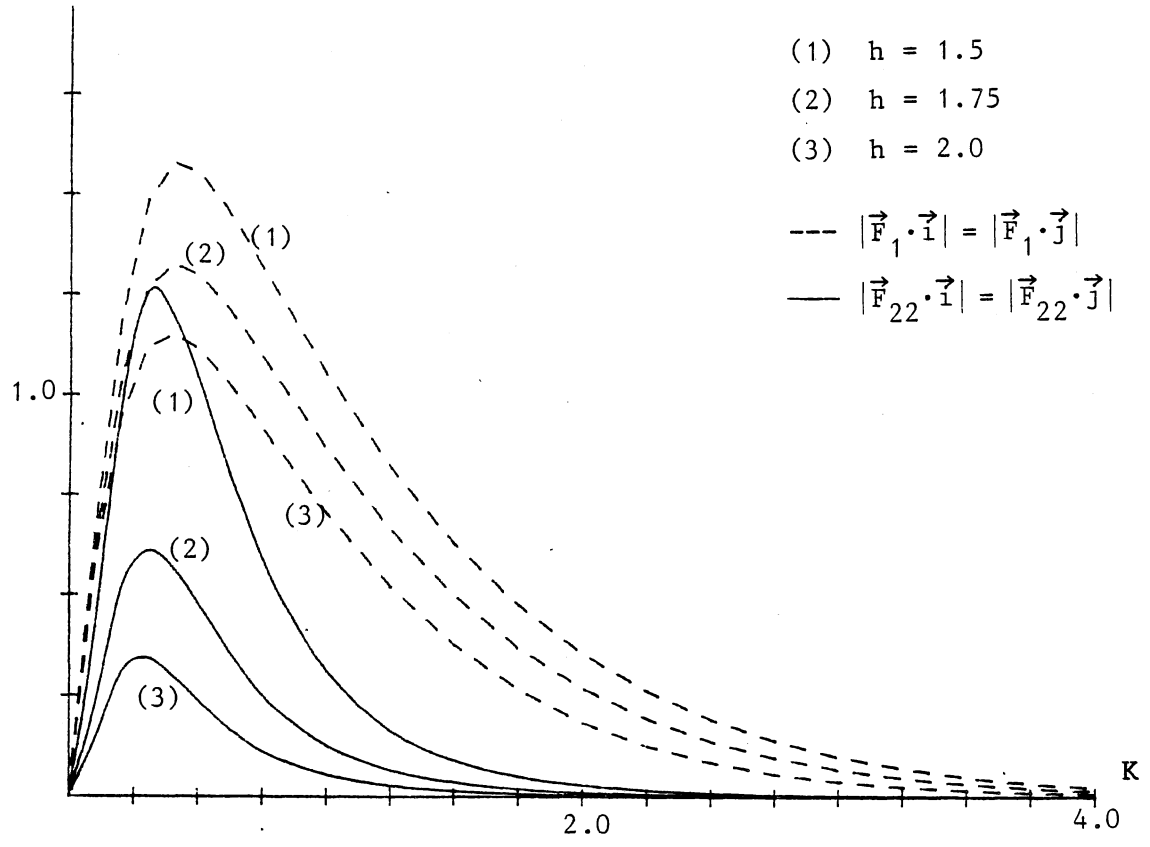


Fig. 6. The first-order (dotted) and second-order (full line) oscillatory forces on the circle.

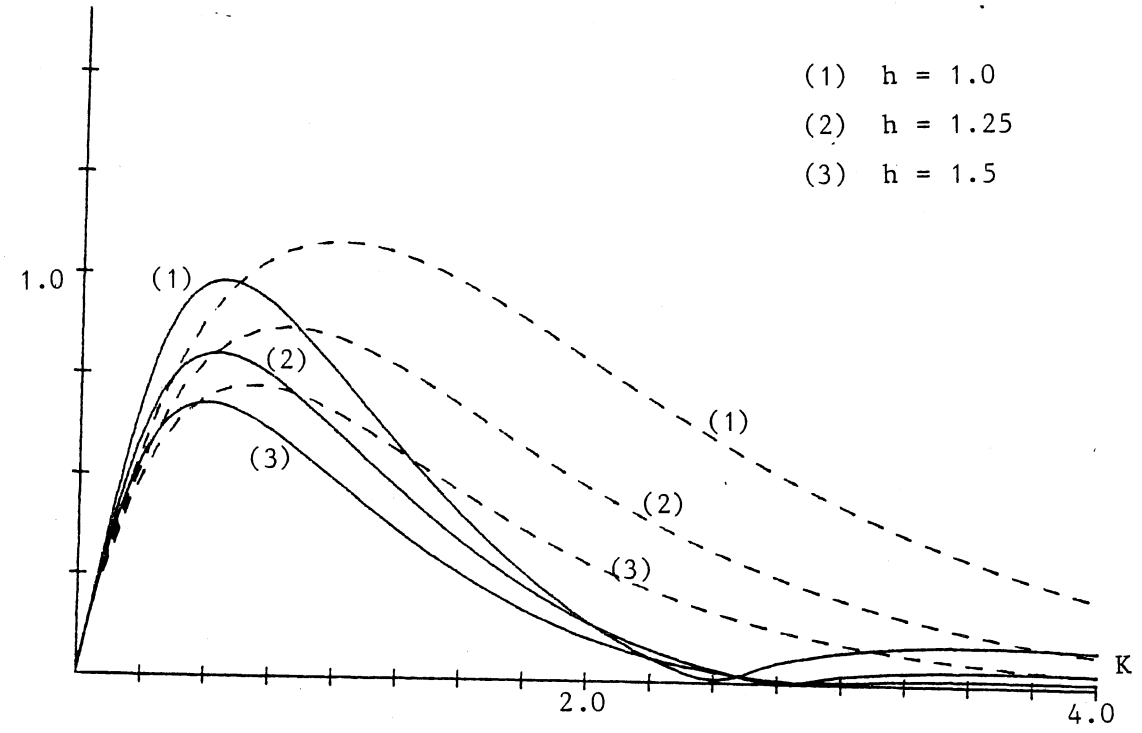


Fig. 7. Horizontal first-order force on the pontoon.
Dotted: Morrison's formula.

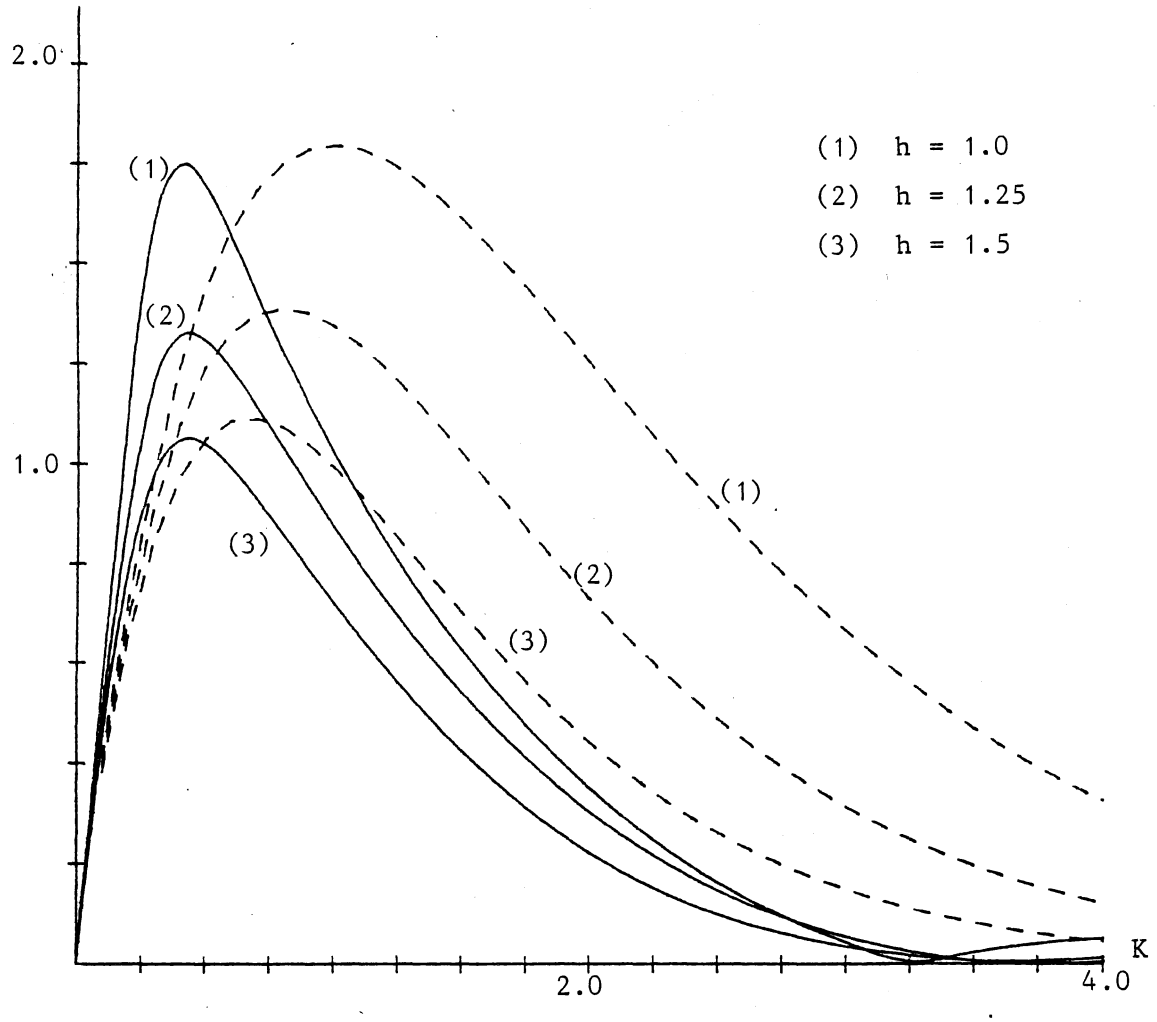


Fig. 8. Vertical first-order force on the pontoon.
Dotted: Morrison's formula.

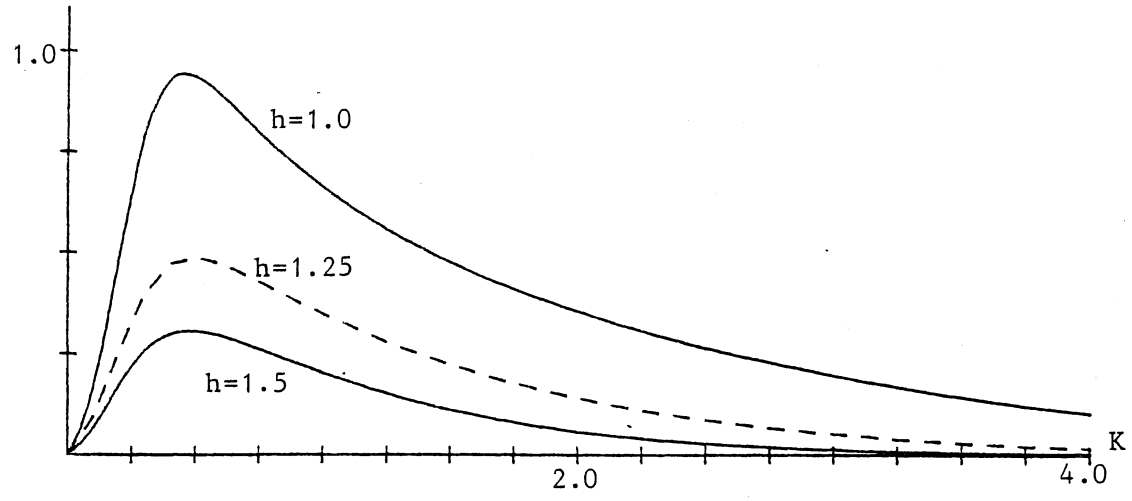


Fig. 9. Mean vertical force on the pontoon.

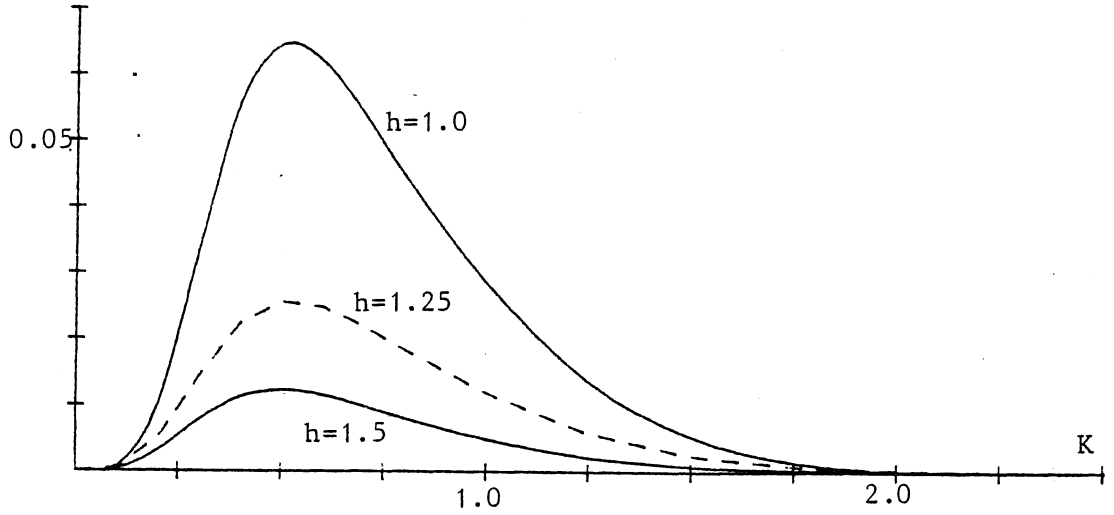


Fig. 10. Mean horizontal force on the pontoon.

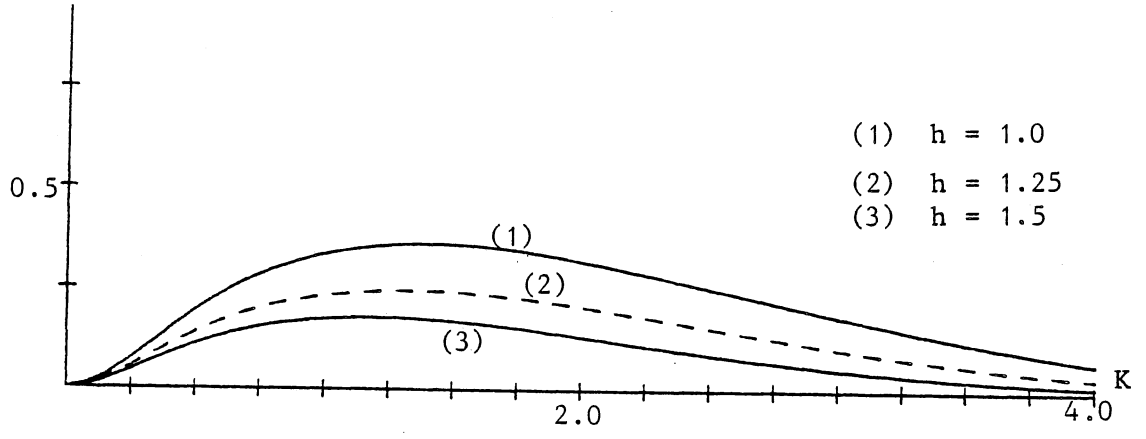


Fig. 11. First-order moment on the pontoon.

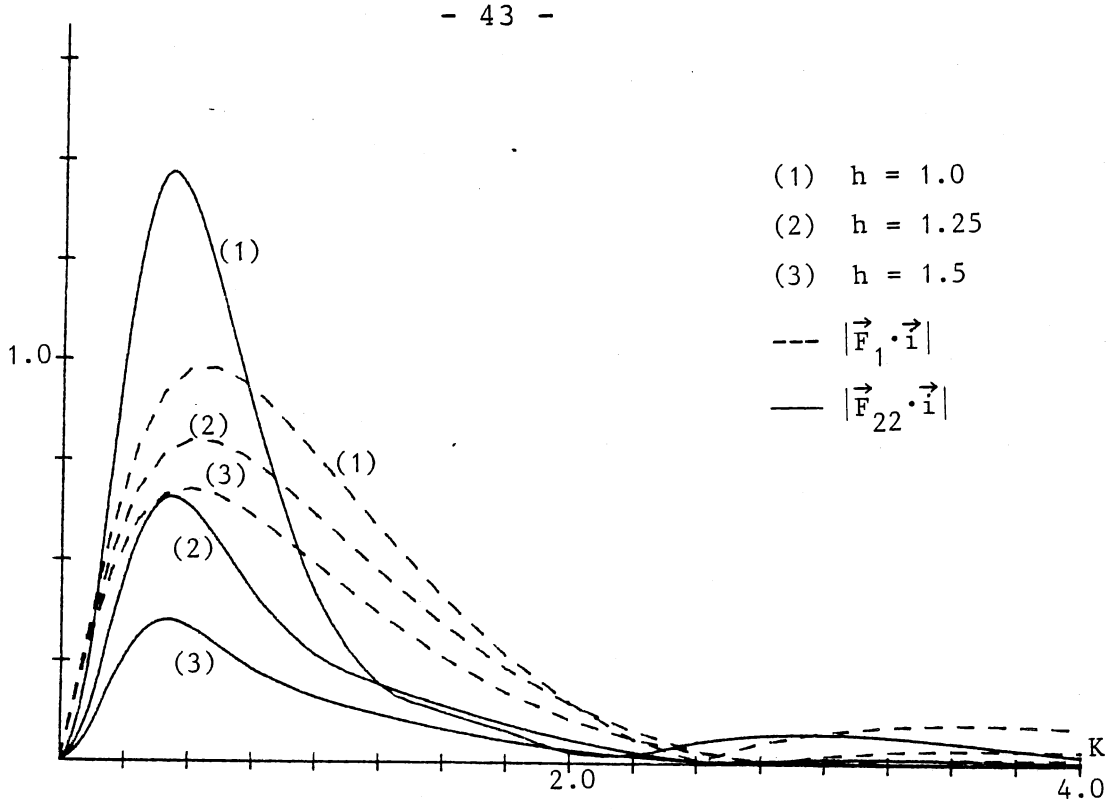


Fig. 12. Second-order oscillatory horizontal force on the pontoon. Dotted line: First-order force.

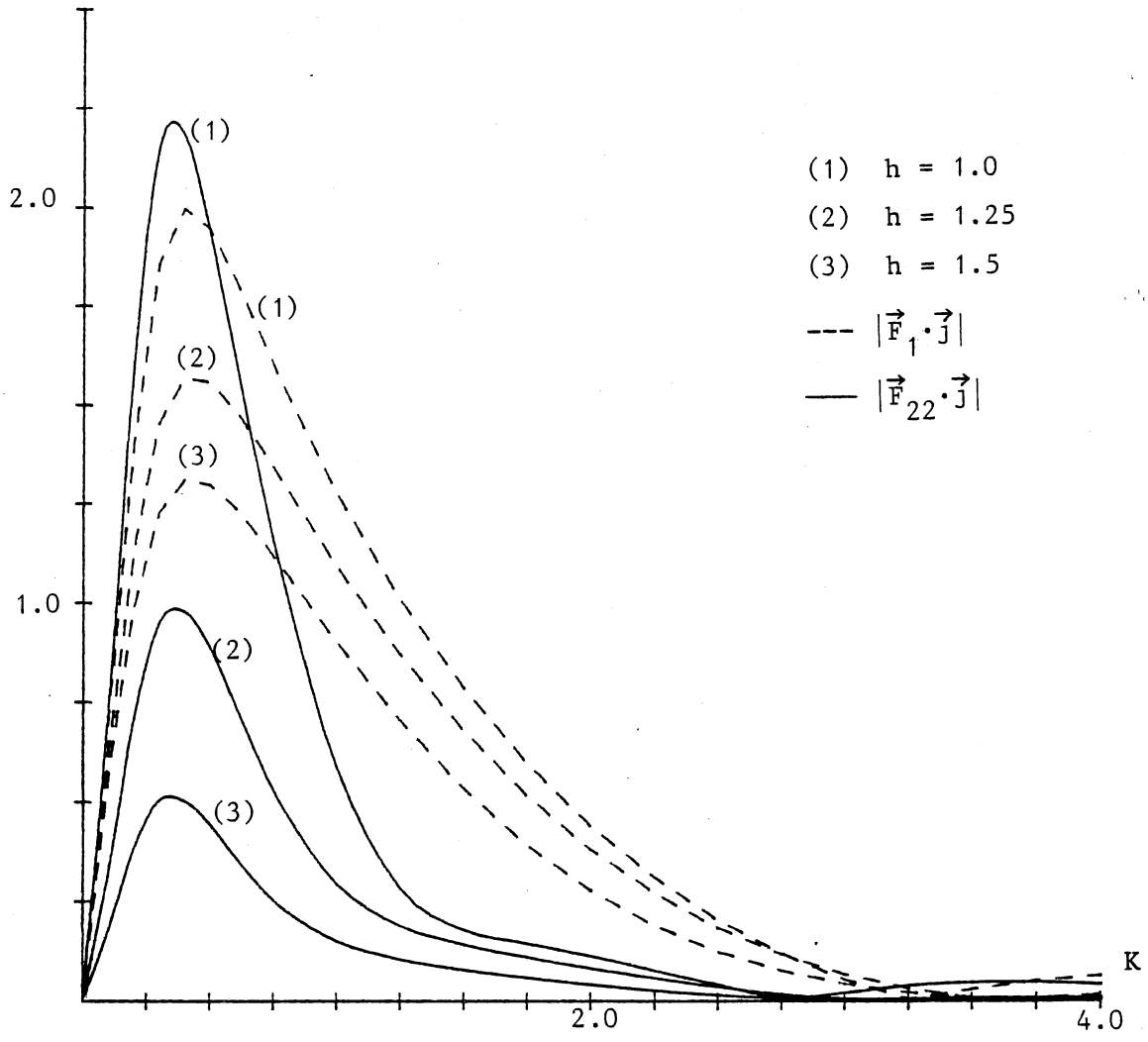


Fig. 13. Second-order oscillatory vertical force on the pontoon. Dotted line: First-order force.

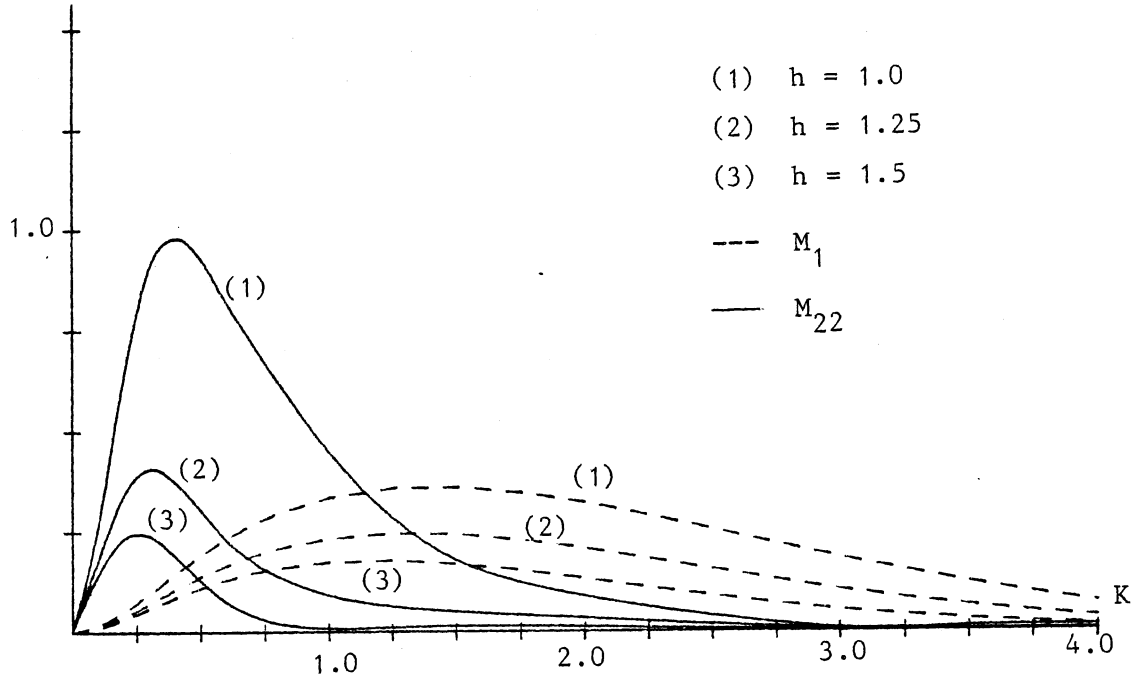


Fig. 14. Second-order oscillatory moment on the pontoon. Dotted line: First-order moment.

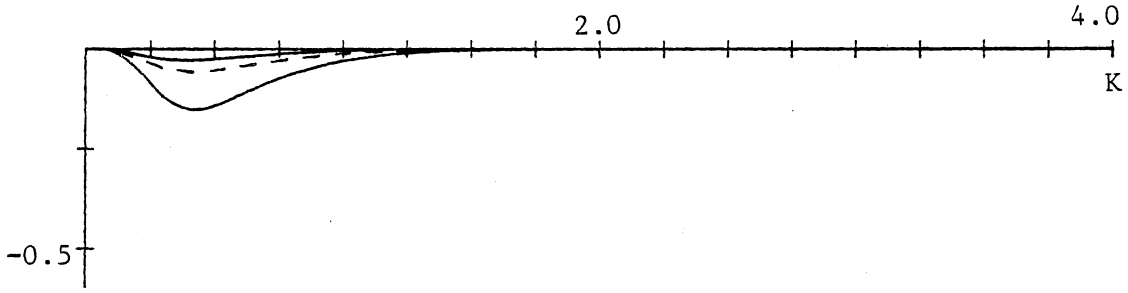


Fig. 15. Mean moment on the pontoon.

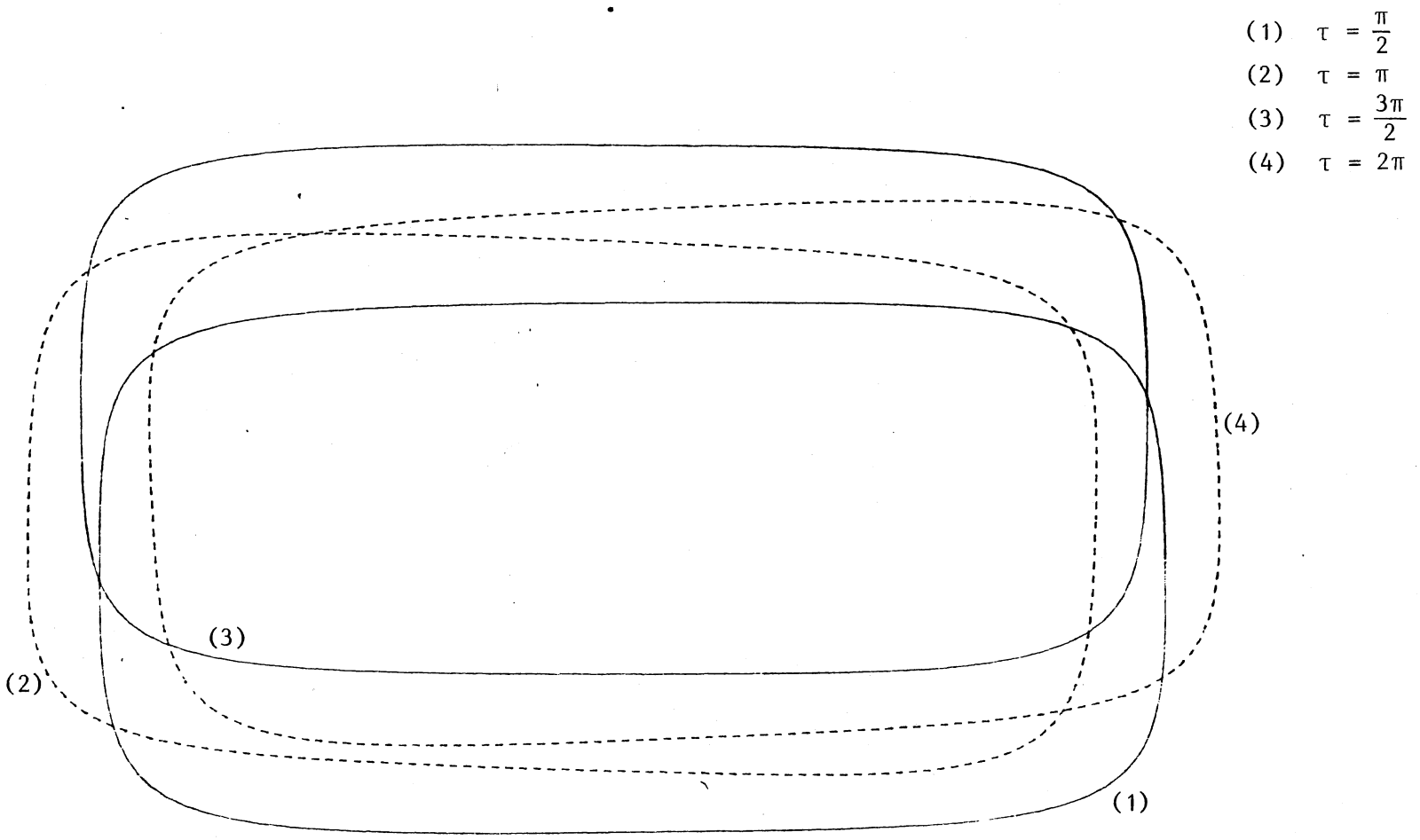


Fig. 16. First-order motion of a neutrally buoyant, freely floating pontoon. $K = 0.5$, $h = 1.0$, $\varepsilon = 0.3$. The upper line indicates the mean free surface.

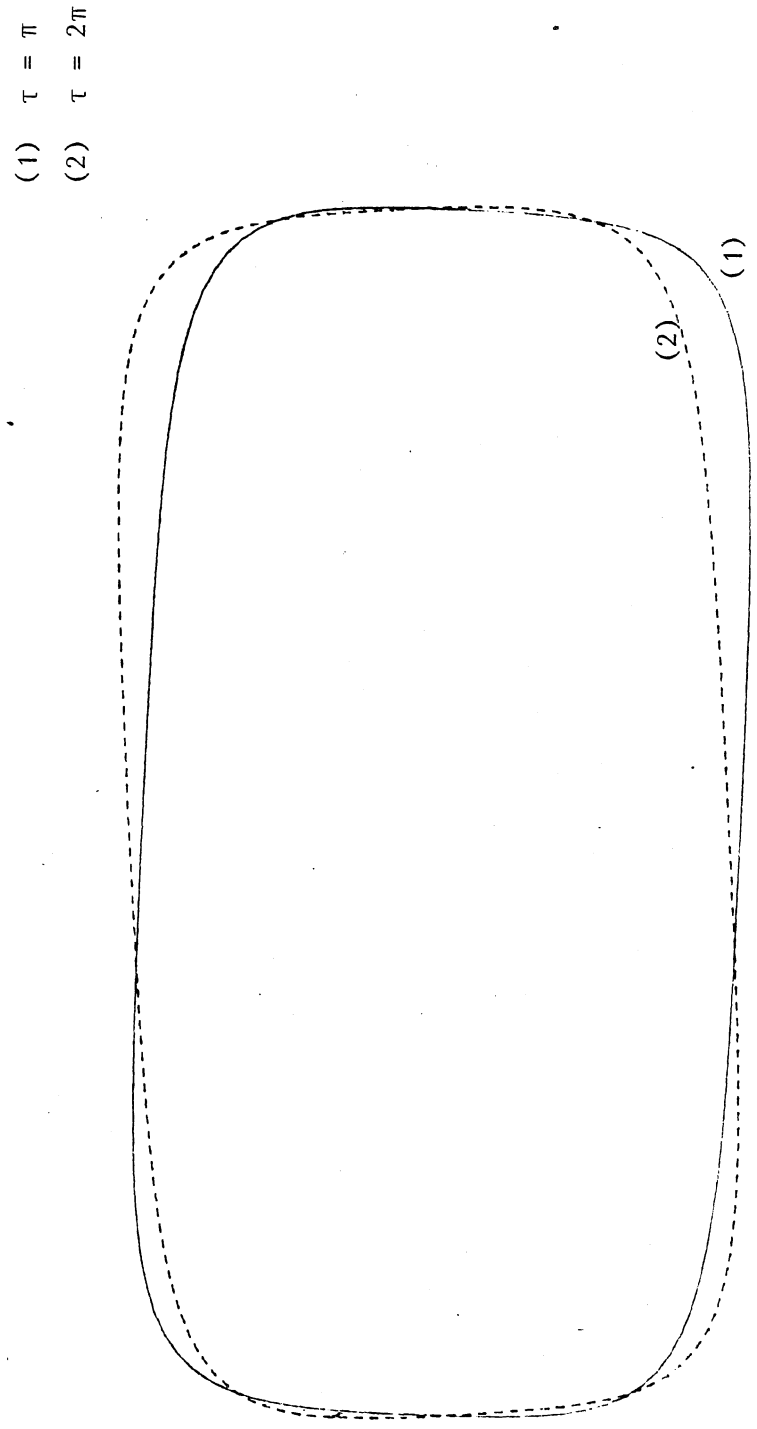


Fig. 17. As fig. 16, but with K = 2.5.

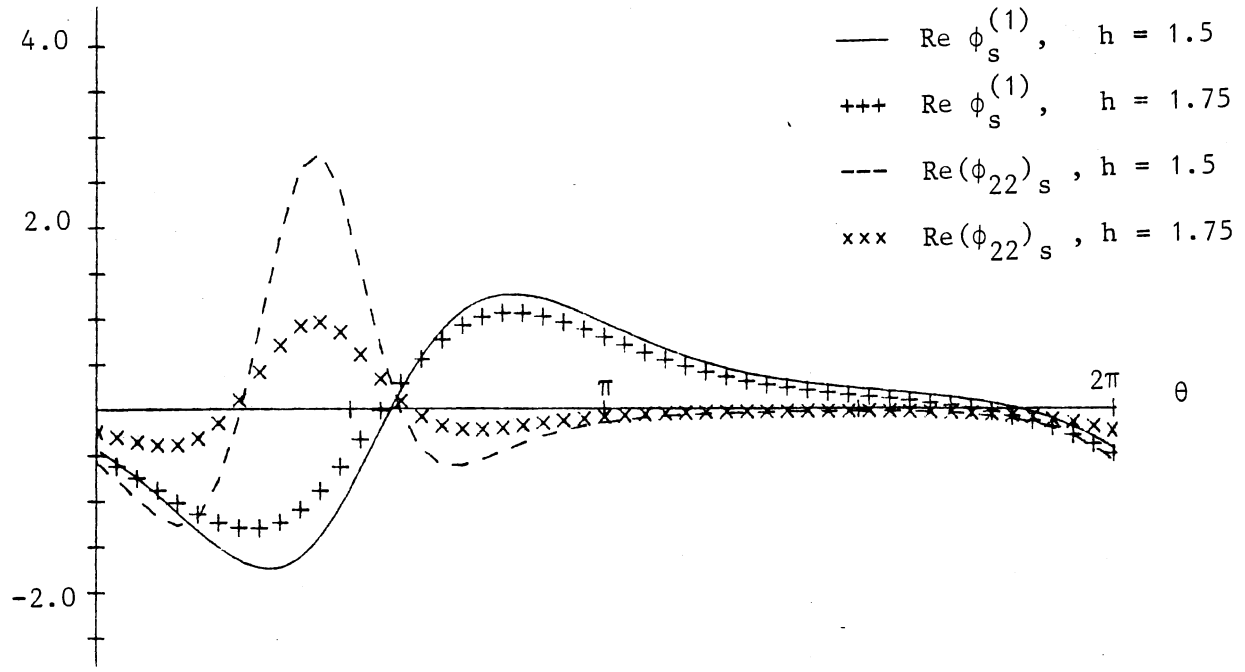


Fig. 18. The tangential velocity on the circle for $\tau = 0$, $K = 0.5$.

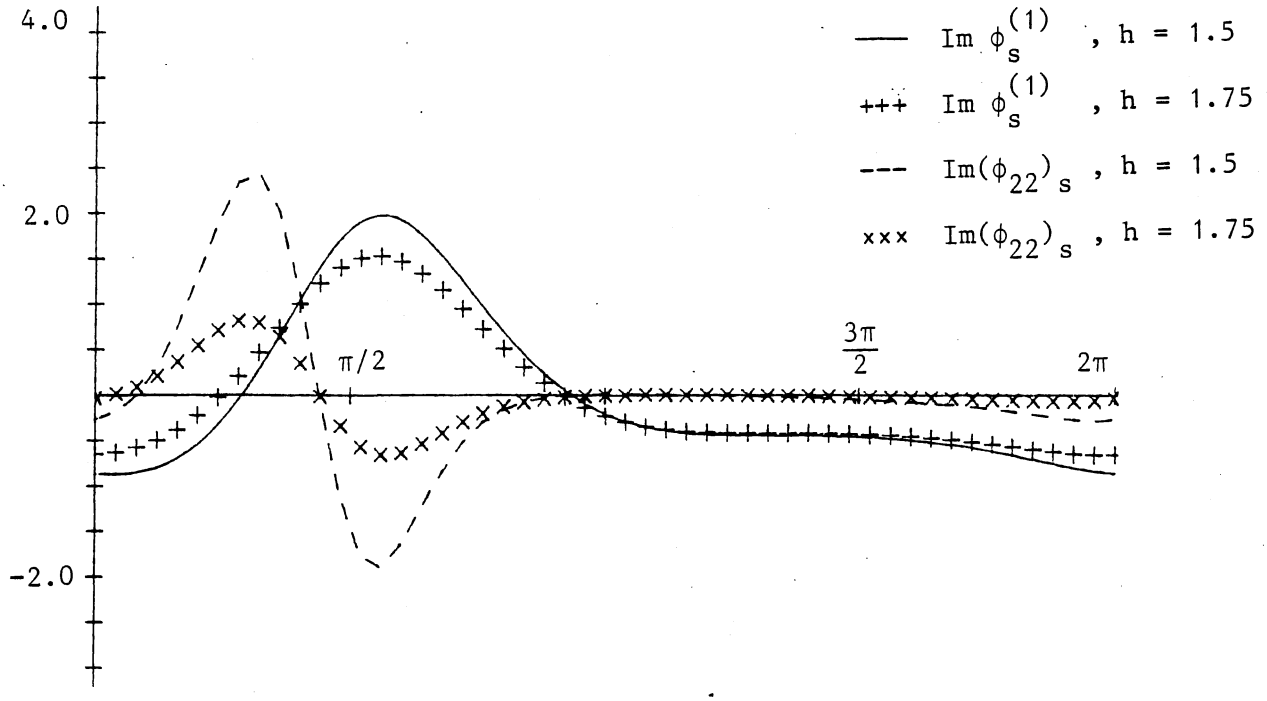


Fig. 19. The tangential velocity on the circle for $\tau = \pi/2$, $K = 0.5$.

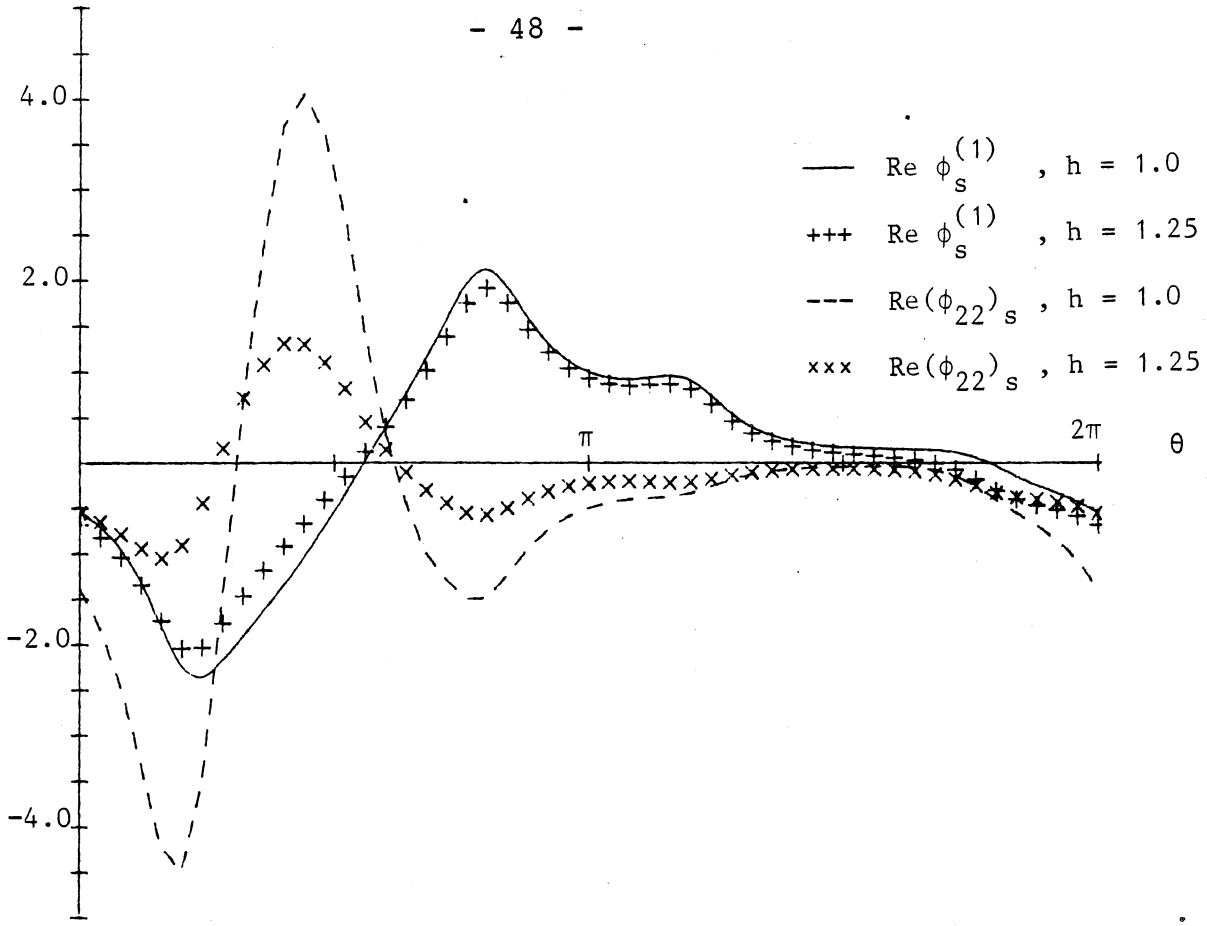


Fig. 20. The tangential velocity on the pontoon for $\tau = 0$, $K = 0.5$

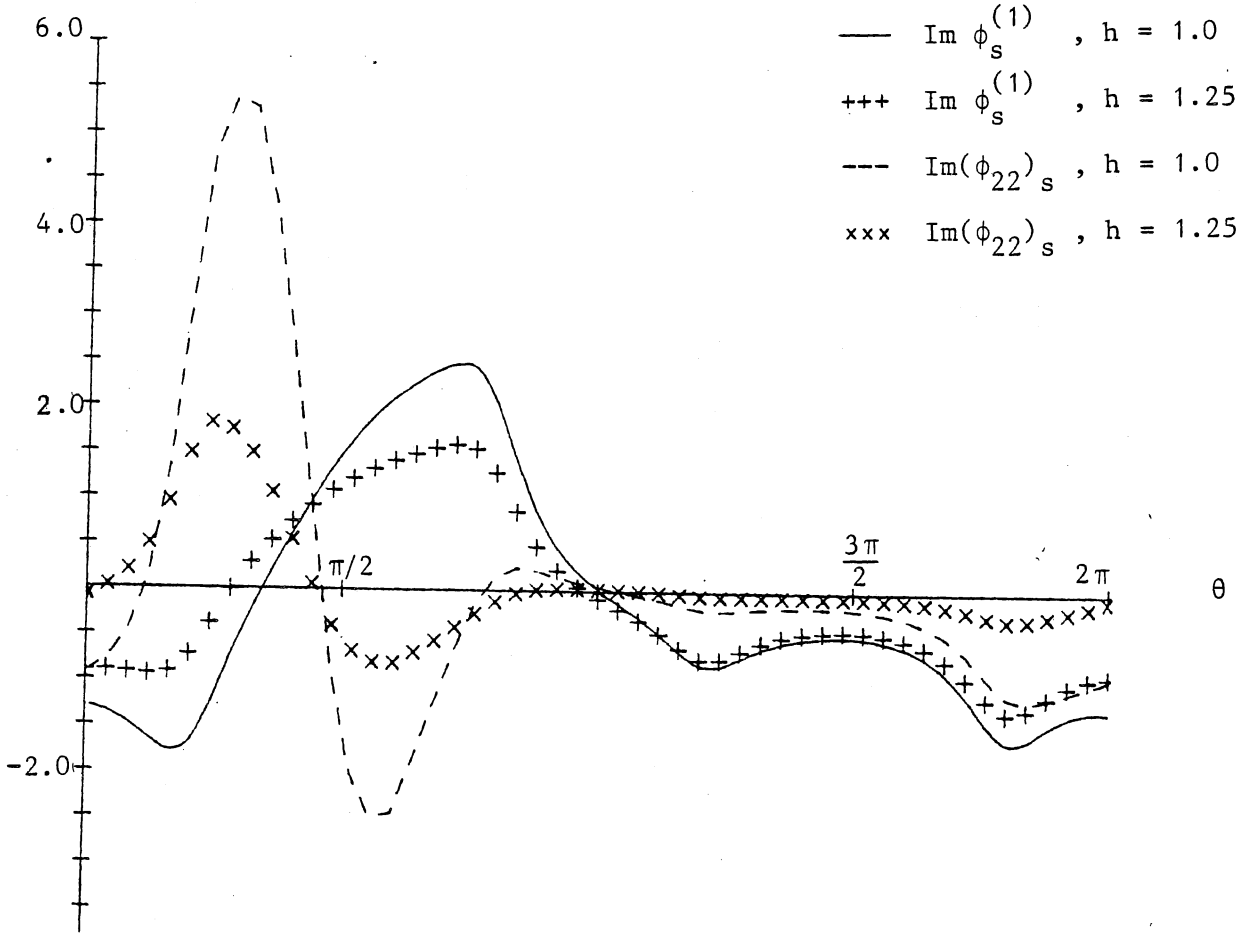


Fig. 21. The tangential velocity on the pontoon for $\tau = \pi/2$, $K = 0.5$.

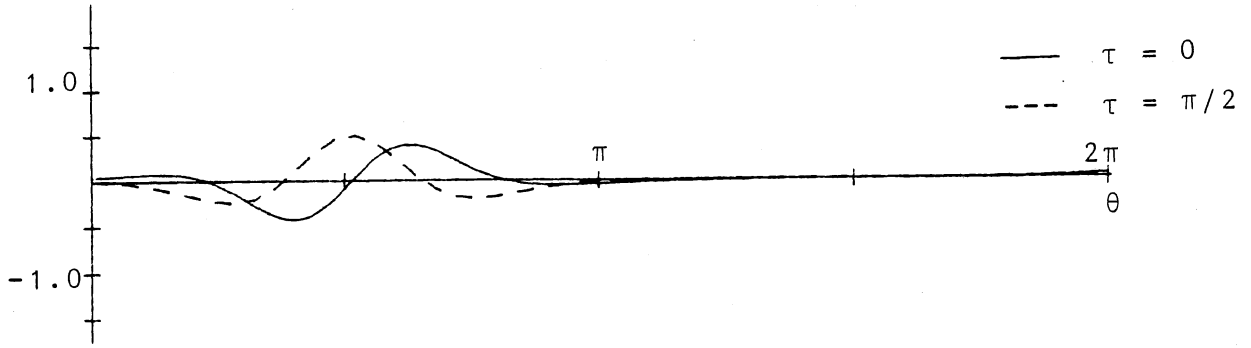


Fig. 22. First-order tangential velocity on the circle for K = 2.5, h = 1.5.

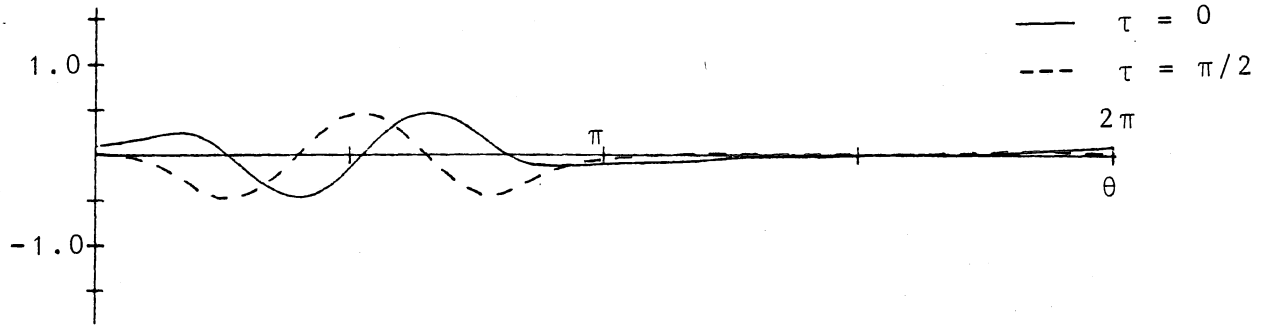


Fig. 23. First-order tangential velocity on the pontoon for K = 2.5, h = 1.0.

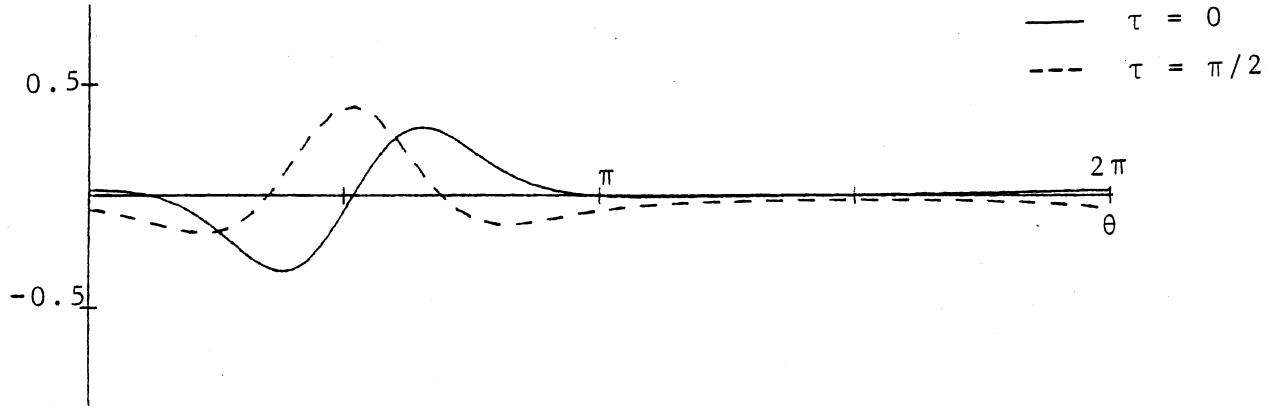


Fig. 24. First-order pressure on the circle for K = 2.5, h = 1.5.

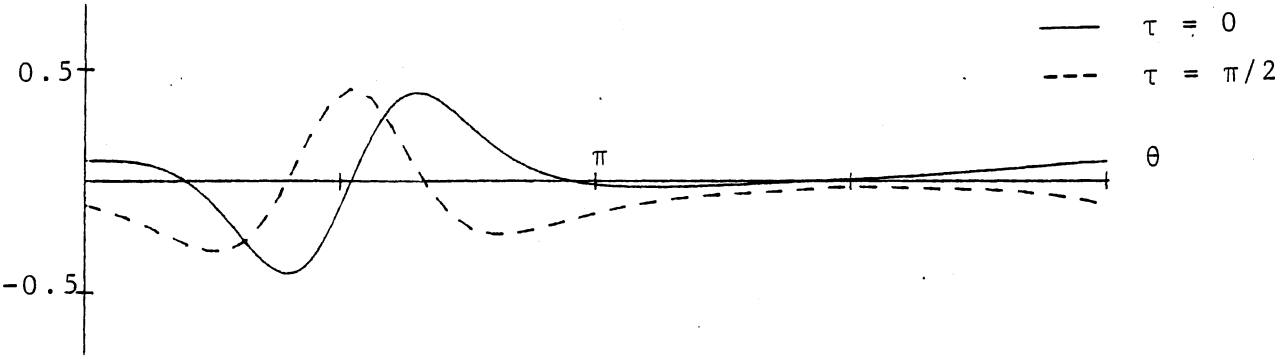


Fig. 25. First-order pressure on the pontoon for K = 2.5, h = 1.0.

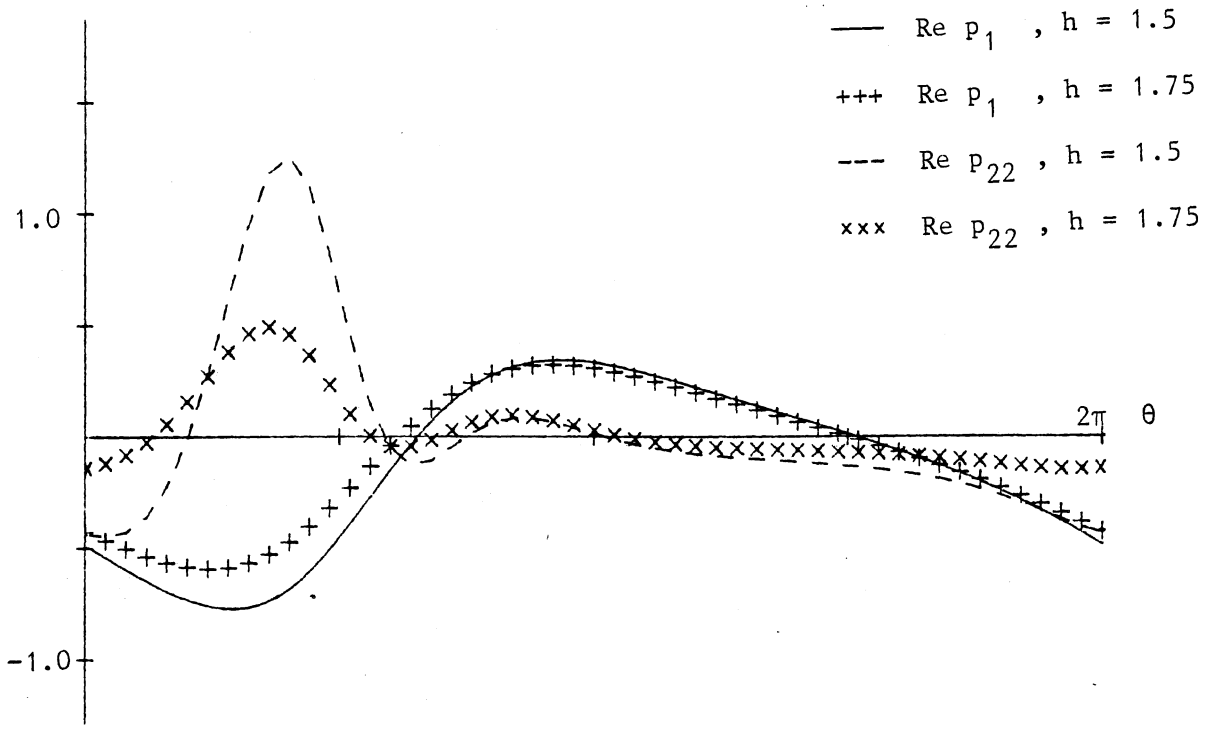


Fig. 26. The oscillatory pressure on the circle for $\tau = 0$, $K = 0.5$.

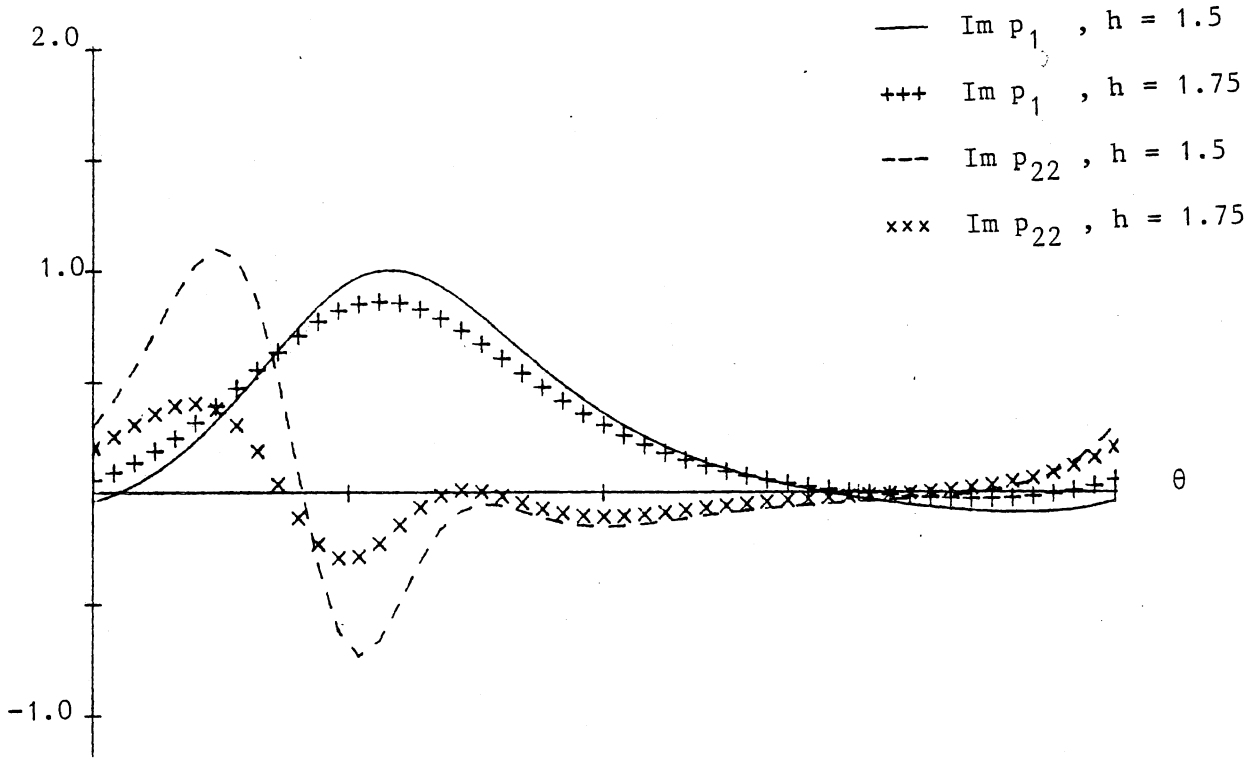


Fig. 27. The oscillatory pressure on the circle for $\tau = \pi/2$, $K = 0.5$.

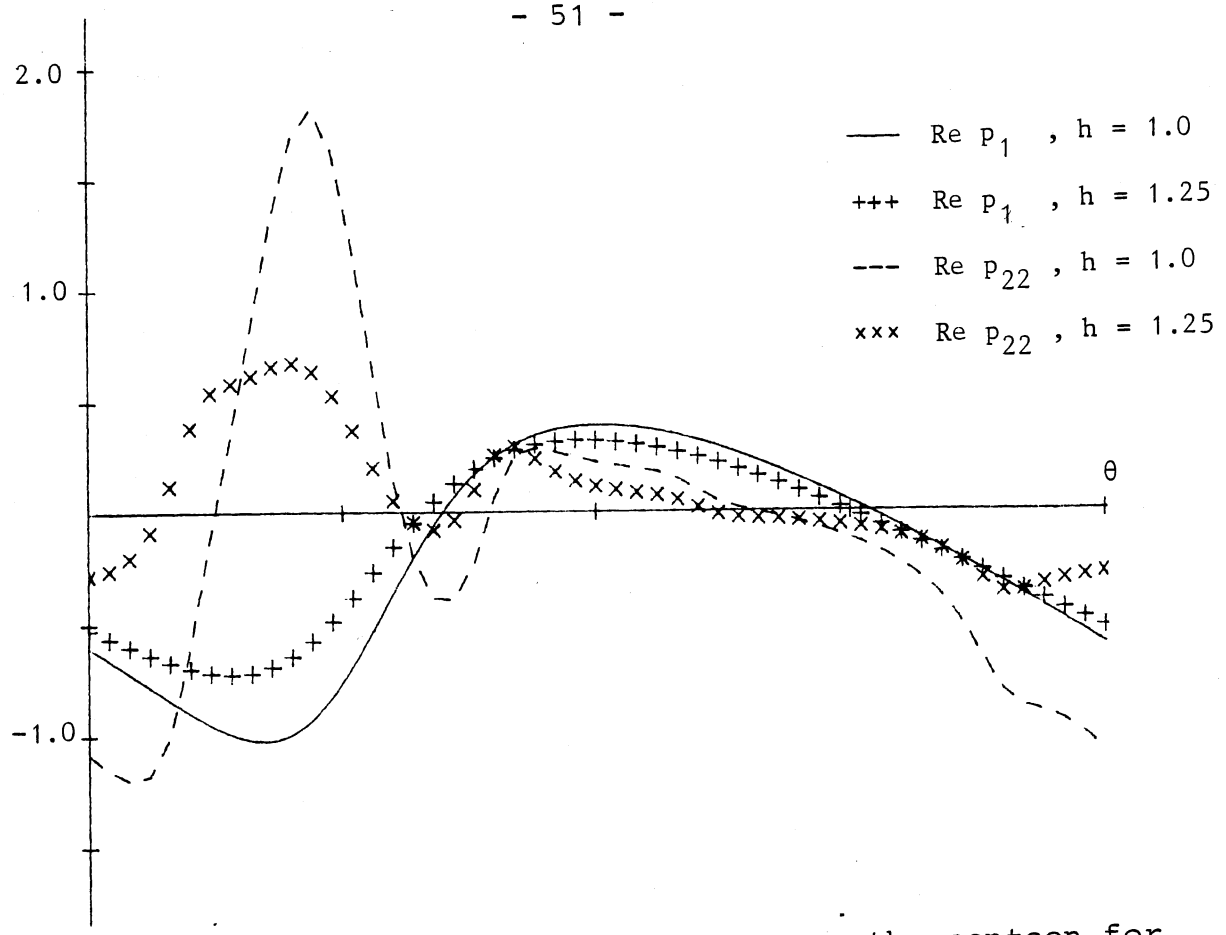


Fig. 28. The oscillatory pressure on the pontoon for $\tau = 0$, $K = 0.5$.

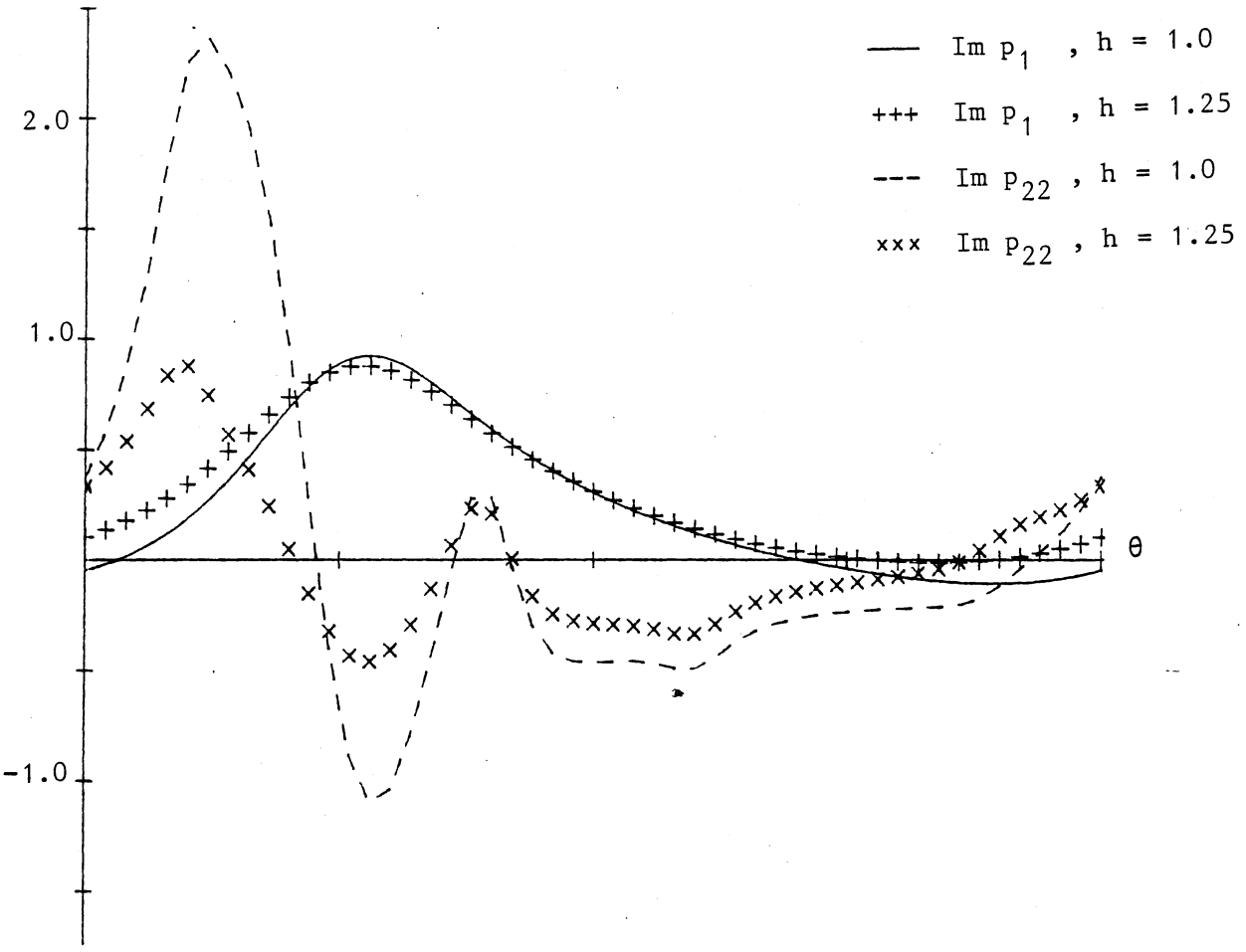


Fig. 29. The oscillatory pressure on the pontoon for $\tau = \pi/2$, $K = 0.5$

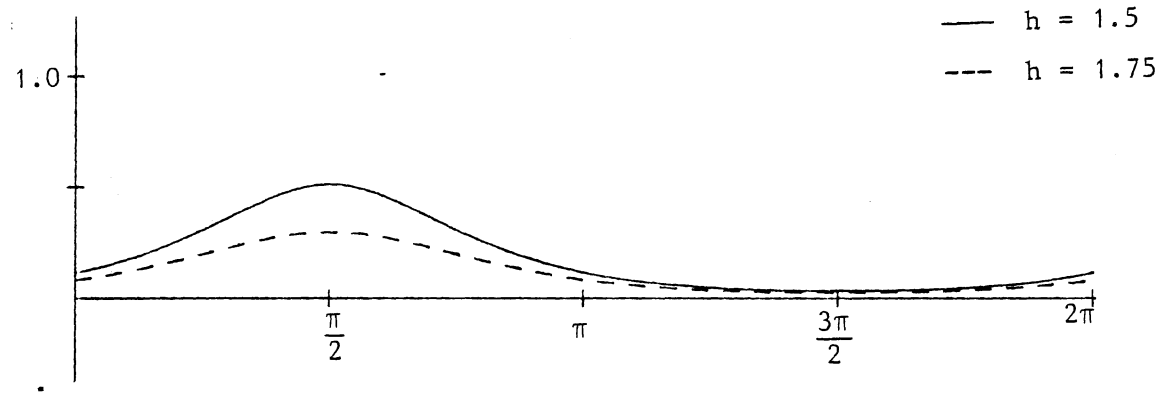


Fig. 30. The mean pressure on the circle for K = 0.5.

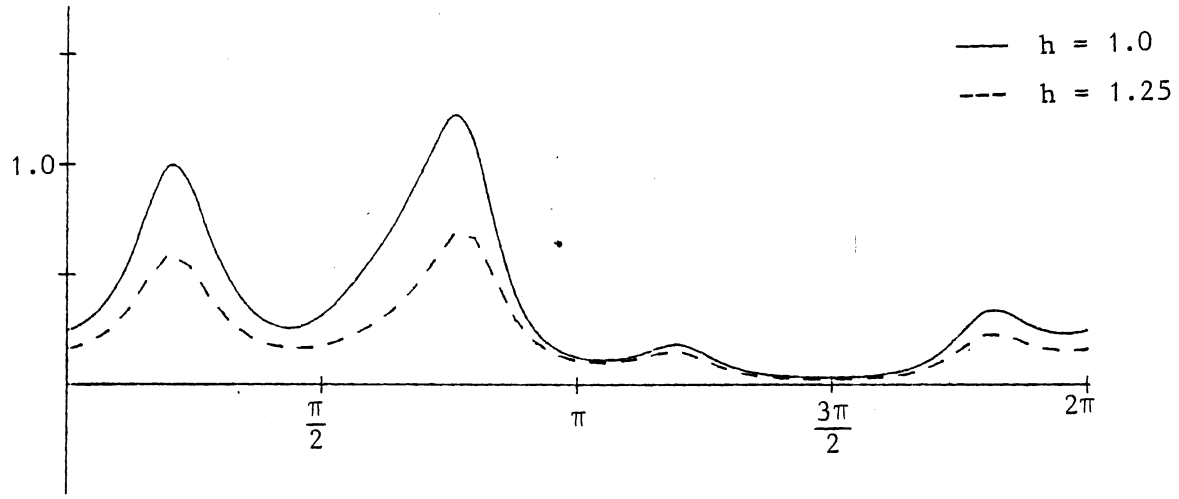


Fig. 31. The mean pressure on the pontoon for K = 0.5.

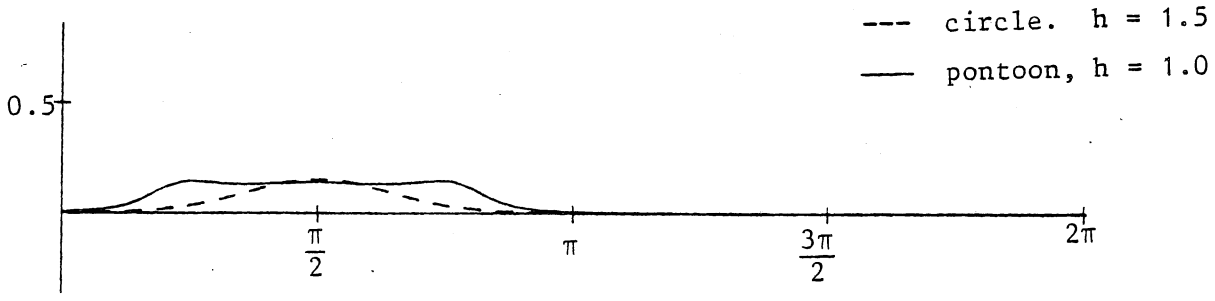


Fig. 32. The mean pressure for K = 2.5

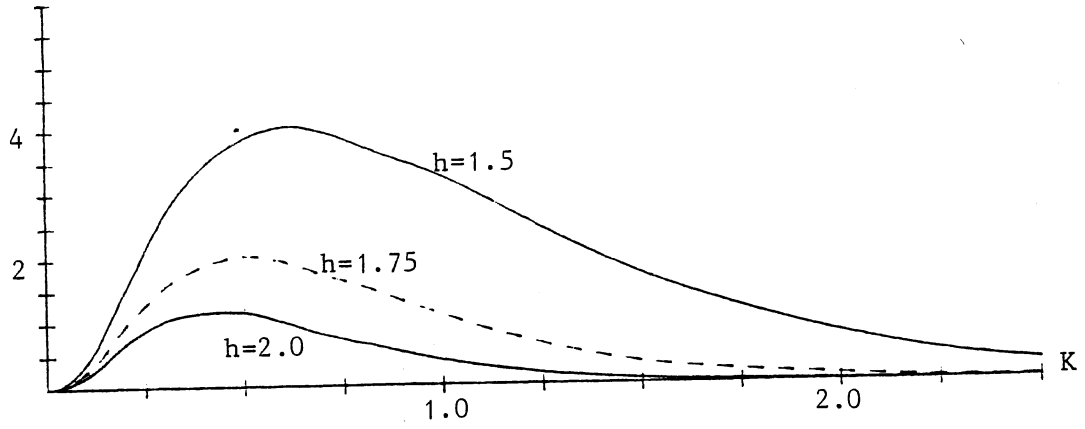


Fig. 33. The second order transmission coefficient, $T_2$, for the circle ($T_1 \equiv 1.0$).

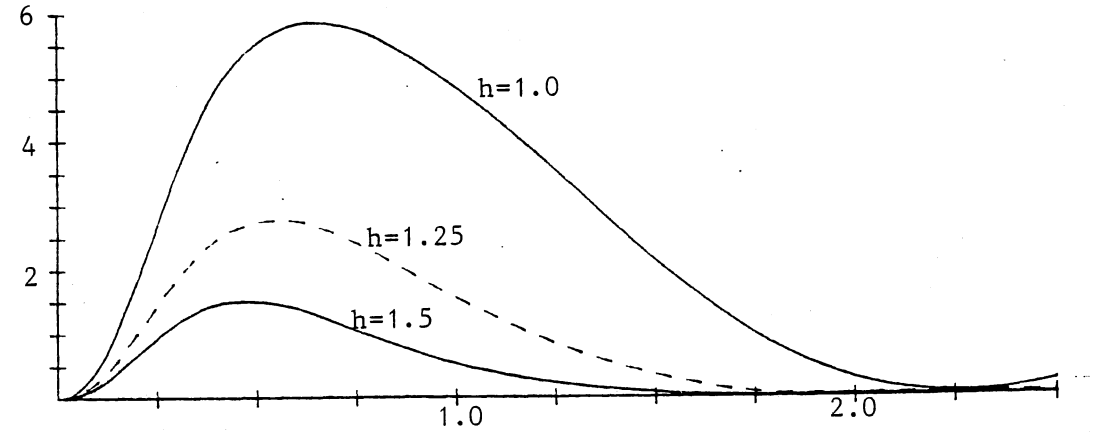


Fig. 34. $T_2$ for the pontoon. ($T_1 \approx 1.0$).

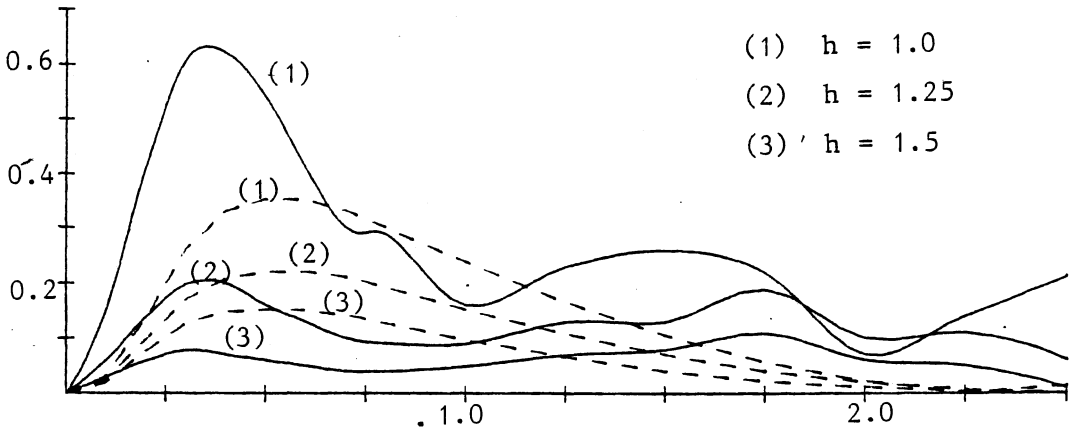


Fig. 35. First- and second-order reflection coefficient for the pontoon. Dotted line: $R_1$, full line: $R_2$

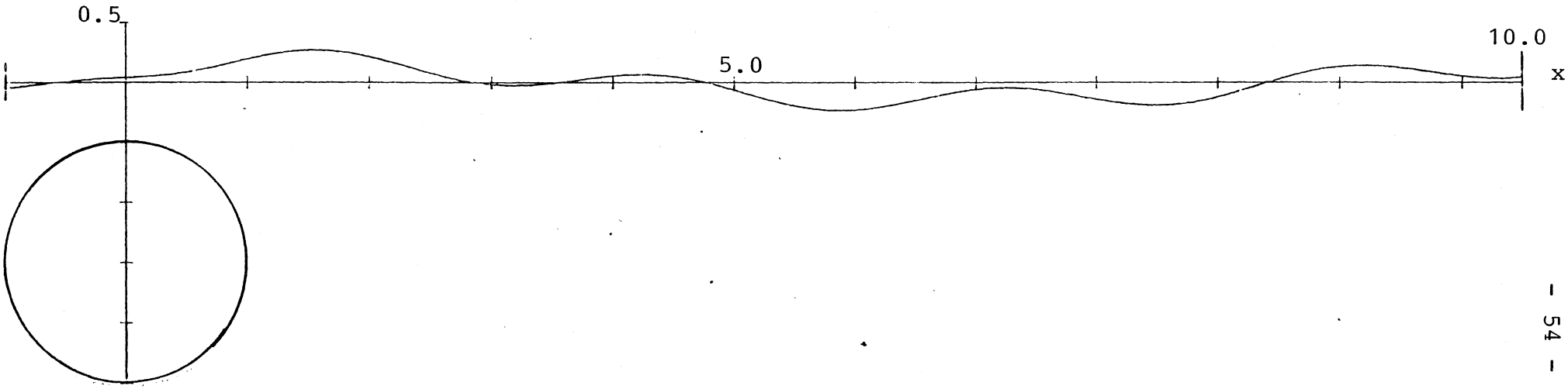


Fig. 36. The surface elevation in natural scale for $K = 0.56$, $\varepsilon = 0.16$, $h = 1.5$, $\tau = 0$.

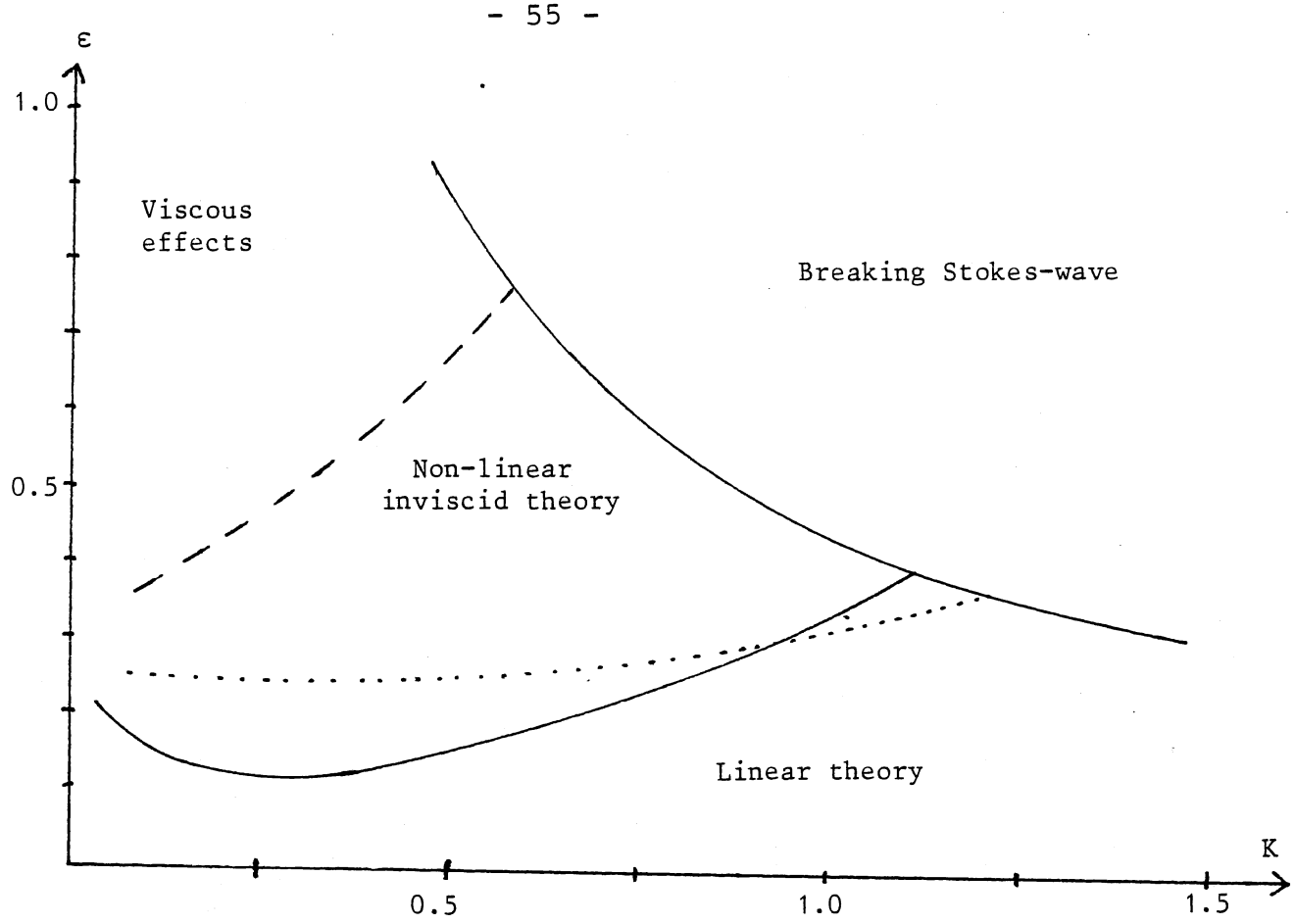


Fig. 37. The different regimes for the circle with h = 1.5.

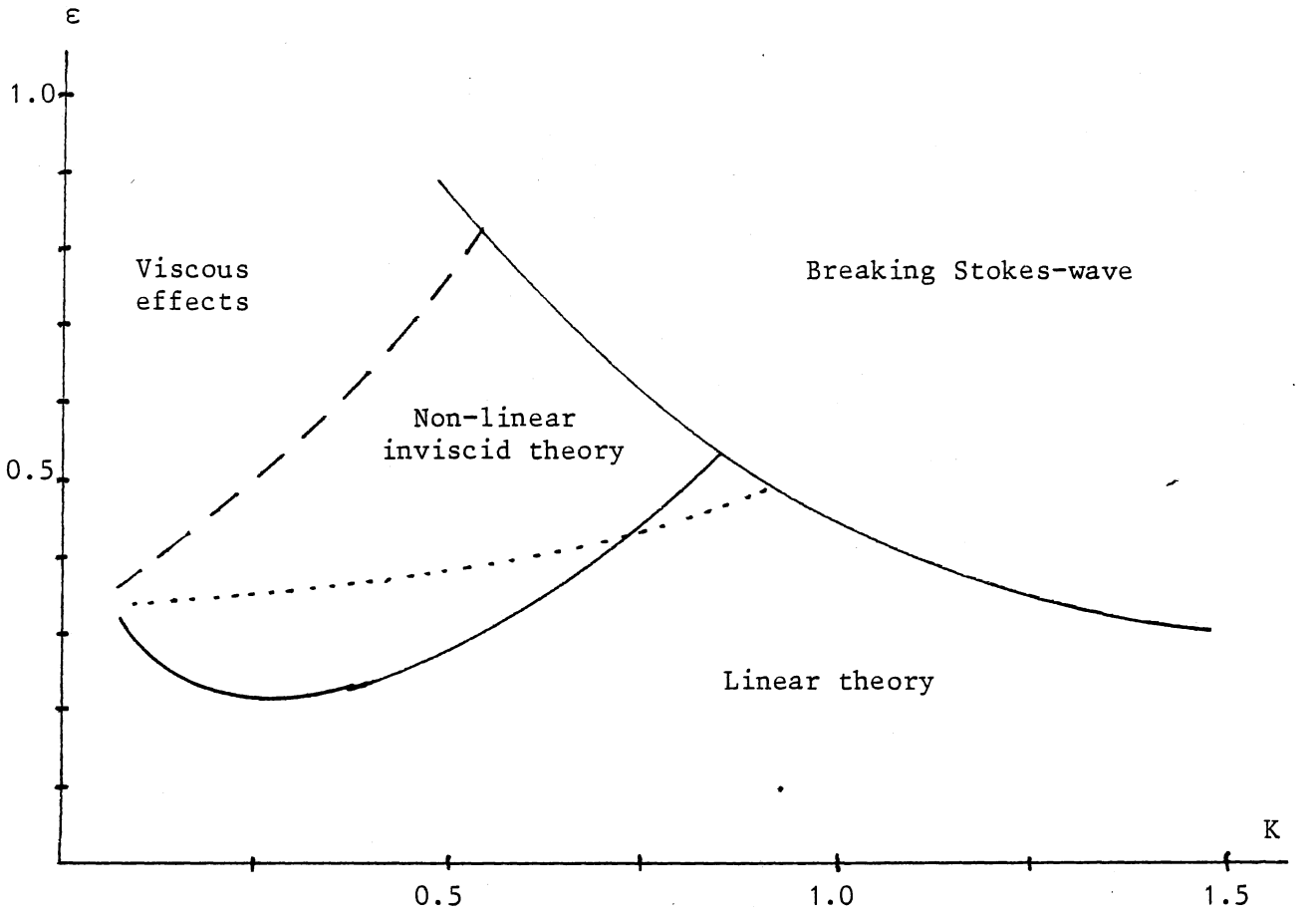


Fig.38. Circle, h = 1.75.

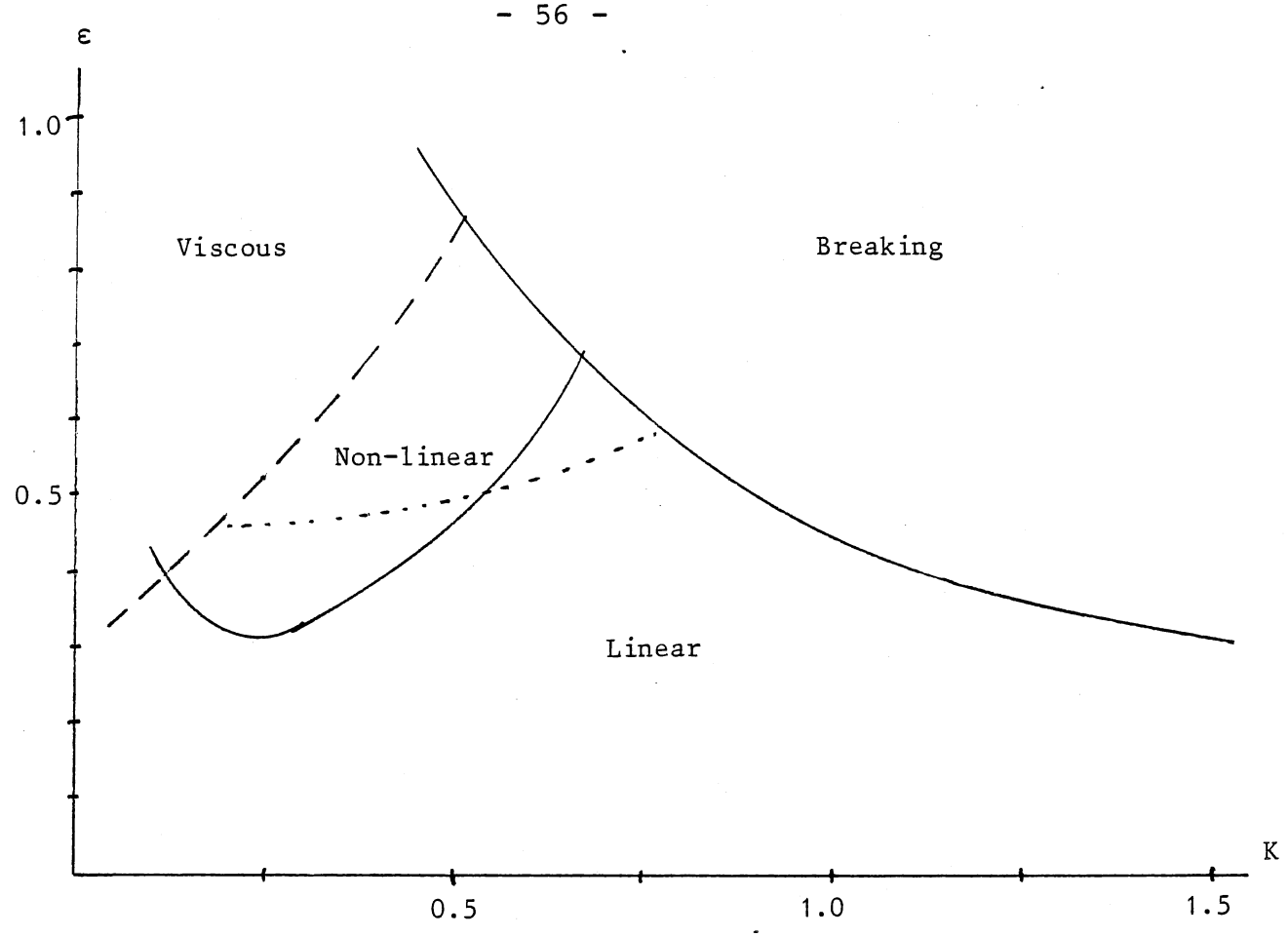


Fig. 39. Circle, h = 2.0.

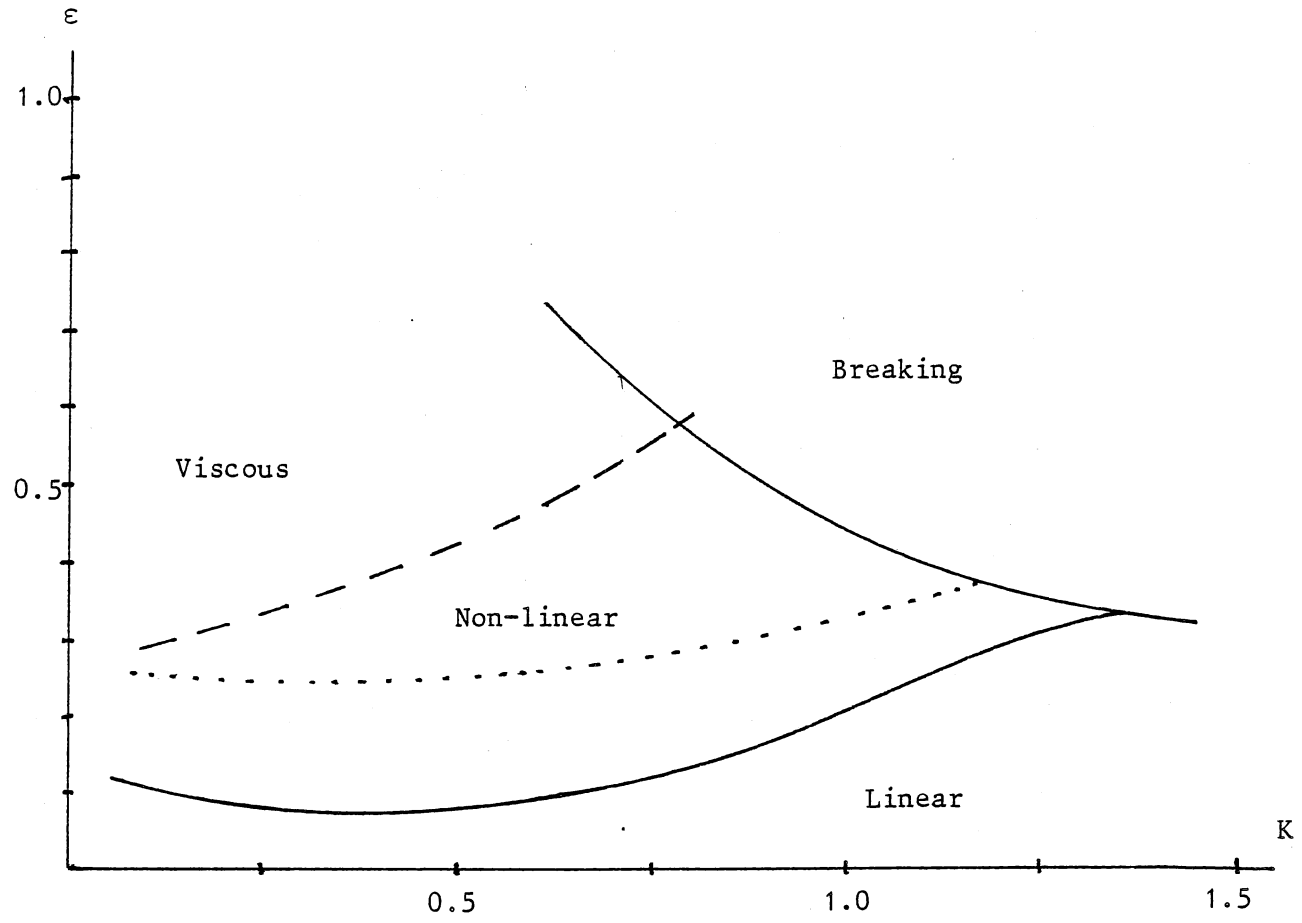


Fig. 40. Pontoon, h = 1.0.

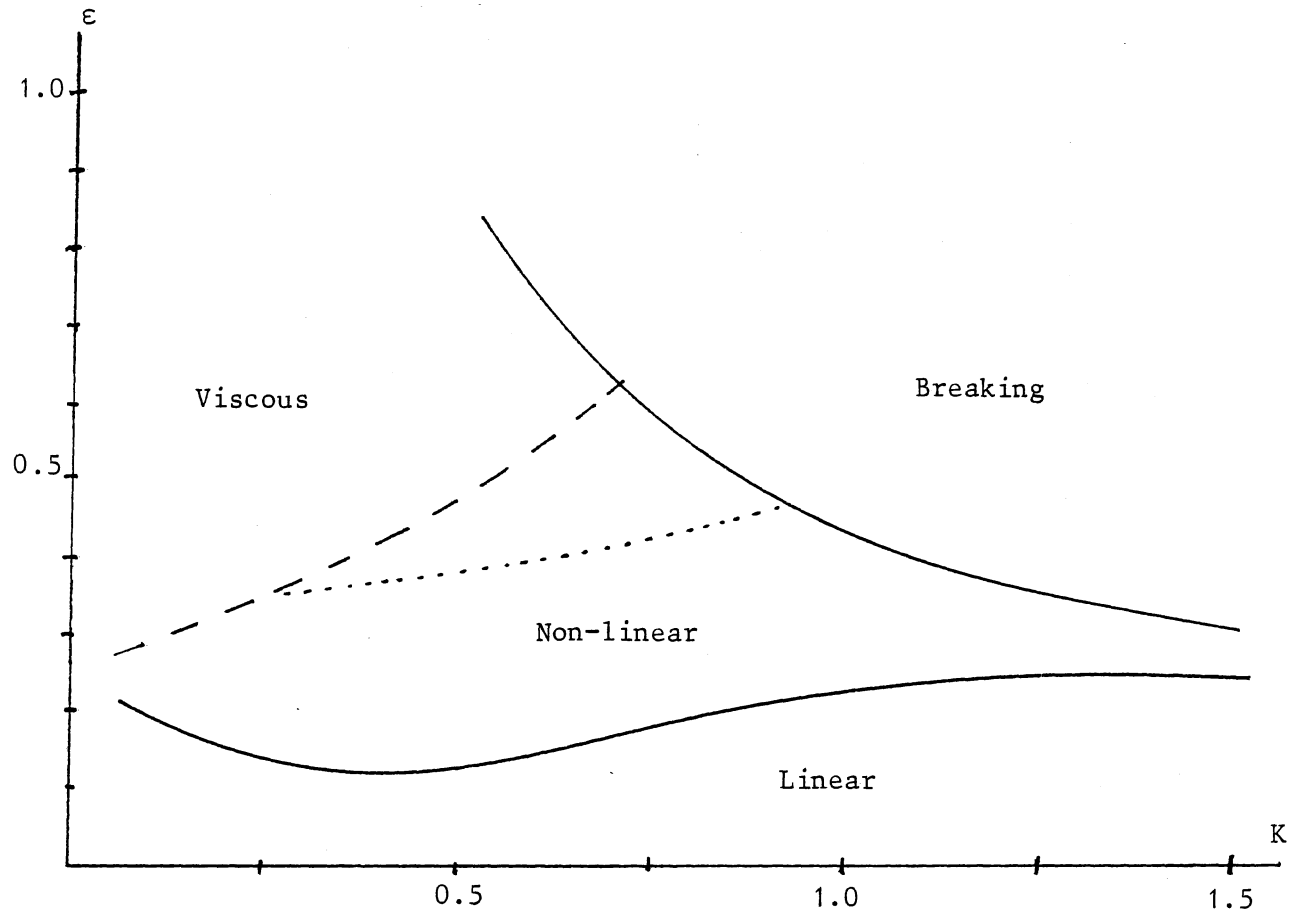


Fig. 41. Pontoon, h = 1.25.

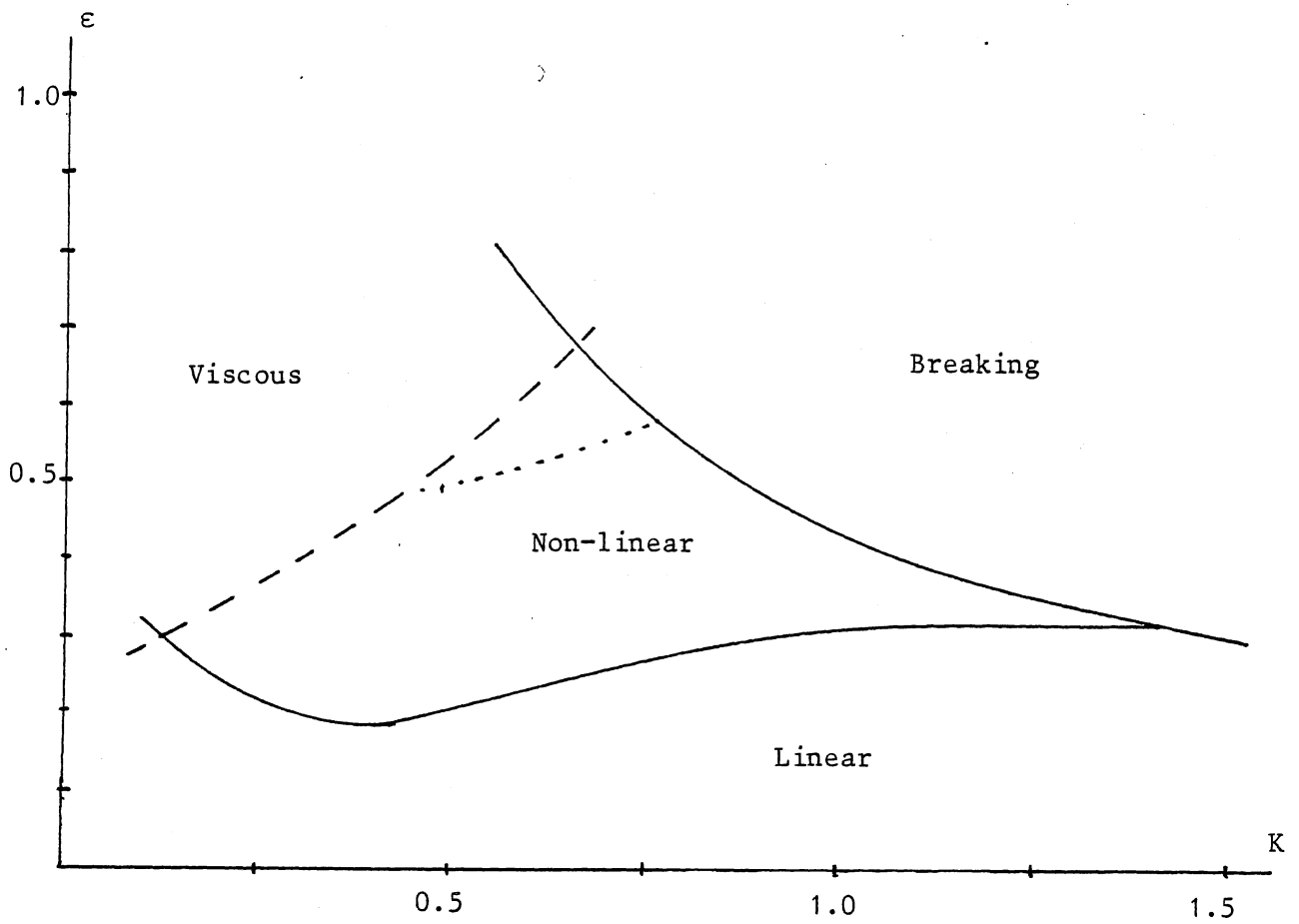


Fig. 42. Pontoon, h = 1.5.

## APPENDIX A. COMPUTATION OF THE SPLINES

The B-splines are piecewise cubic polynomials which satisfy the following conditions:

1. $B_i(\theta) = 0 \quad \theta \leqslant \theta_{i-2}$ or $\theta \geqslant \theta_{i+2}$
2. $B_i(\theta) > 0 \quad \theta_{i-2} < \theta < \theta_{i+2}$
3. $B_i'(\theta)$ and $B_i''(\theta)$ are continuous for all $\theta$
4. If $\theta \in [x_{i-1}, x_i]$ then $\sum_{j=i-2}^{i+1} B_i(\theta) = 1$

An example is shown in the following figure:

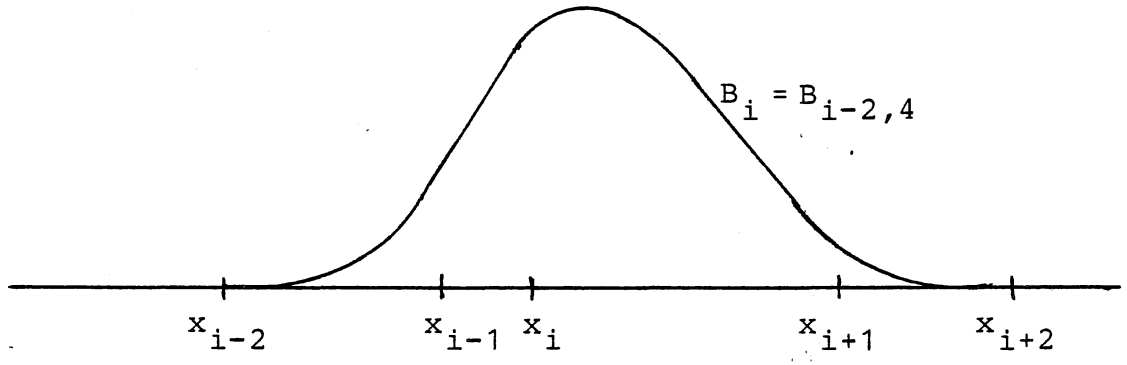


The shape of the spline depends only weakly on the choice of $x_{i-1}, x_i$ and $x_{i+1}$. The explicit form of the polynomials will be a rather complicated expression but the value can be easily computed from the recurrence relation

$$B_{j,1}(x) = \begin{cases} 1 & x_j \leqslant x < x_{j+1} \\ 0 & \text{otherwise} \end{cases}$$

$$B_{i,k}(x) = \frac{x - x_i}{x_{i+k-1} - x_i} B_{i,k-1}(x) + \frac{x_{i+k} - x}{x_{i+k} - x_{i+1}} B_{i+1,k-1} \quad , \quad k > 1$$

This is a sum of positive quantities only which can be evaluated without loss of numerical accuracy. The relation is taken from de Boor [7] and the two-index notation is due to his work.

If the points $x_i$ are a given partition of an interval $[a,b]$ such that

$$a = x_1 < x_2 < \ldots < x_{N-1} < x_N = b$$

then $B_1, B_2, \ldots, B_N$ will form a basis for all piecewise cubic polynomials with two continuous derivatives on this interval with the given partition. Hence all these functions can be written as

$$p(x) = \sum_{i=1}^{N} \alpha_i B_i(x)$$

## APPENDIX B. AN ALTERNATIVE COMPUTATION OF THE SECOND-ORDER FORCE

Applying Green's theorem it is possible to compute $M_{22}$ and $\vec{F}_{22}$ without the solution of the $\phi_{22}$-problem. Instead, a set of first-order problems must be solved.

We first introduce the first-order radiation potentials for an oscillation with frequency $2\omega$. These potentials are the solutions of

$$\begin{cases} \nabla^2\phi_i = 0 \quad \text{in the fluid} \\ (\phi_i)_n = \begin{cases} n_i & i=1,2 \\ (\vec{r}\times\vec{n})\cdot\vec{k} & i=6 \end{cases} \qquad (x,y)\in C \\ (\phi_i)_y - 4K\phi_i = 0\,, \quad y = 0 \\ (\phi_i)_y = 0\,, \quad y = -\infty \\ (\phi_i)_x \mp 4jK\phi_i = 0, \quad x = \pm\infty \end{cases} \tag{B-1}$$

and can therefore be found in exactly the same way as $\phi_7$, with K replaced by 4K and $-(\phi_0)_n$ replaced by $n_i$ or $(\vec{r}\times\vec{n})\cdot\vec{k}$ in the integral equation (4-7).

If we now put $\alpha = \phi_i$ and $\beta = \phi_{22}$ in Green's theorem, (3-5), we obtain (cfr. fig. 4-1)

$$\int_{\Gamma+C+S_-+B+S_+} (\phi_i \frac{\partial\phi_{22}}{\partial n} - \phi_{22}\frac{\partial\phi_i}{\partial n})ds = 0$$

From (2-10), (2-16), (2-17) and (1) we then get

$$\int_C (\phi_i \frac{\partial\phi_{22}}{\partial n} - \phi_{22}\frac{\partial\phi_i}{\partial n})ds + \int_\Gamma \phi_i(\xi,0)f(\xi)d\xi + \int_{S_-} \phi_i\cdot 4KR_1 ds = 0$$

As in chapter 4 we truncate the integration over $\Gamma$ by setting

$$\int_\Gamma \phi_i(\xi,0)f(\xi)d\xi \approx \int_{x_L}^{x_R} \phi_i(\xi,0)f(\xi)d\xi$$

where $f(\xi)$ is sufficiently small for $\xi > x_R$ and

$$\left.\begin{aligned} f(\xi) &\approx -4KjR_1 \\ \phi_i(\xi,0) &\approx A_i e^{-4Kj\xi} e^{4K\eta} \end{aligned}\right\} \xi < x_L$$

The integral over $S_-$ is then

$$\int_{S_-} \phi_i \cdot 4KR_1 \, ds \approx \int_{-\infty}^{0} A_i e^{-4Kjx_L} e^{4K\eta} \cdot 4KR_1 \, d\eta = A_i R_1 e^{-4Kjx_L}$$

We now have

$$\int_C \phi_{22} \frac{\partial \phi_i}{\partial n} \, ds = -\int_{x_L}^{x_R} \phi_i(\xi,0) f(\xi) d\xi - A_i R_1 e^{-4Kjx_L} \qquad \text{(B-2)}$$

where the right-hand side is independent of $x_L$ if $|x_L|$ is sufficiently large. From the boundary condition on C in (1) we see that the left-hand side in (2) is equal to the first term in (4-17) and (4-18) with the exception of a constant factor $2Kj$. Hence if $\phi_7$ and the radiation potentials for the double frequency, $\phi_i$, are all known, the second-order force and moment can be computed. This method has been used in several works on the second-order radiation problem.

## APPENDIX C. OTHER NUMERICAL CHECKS

We list here some equations which are useful in the check of the various steps of the computation.

Conservation of energy immediately gives

$$R_1^2 + T_1^2 = 1 \tag{C-1}$$

Conservation of momentum gives (see Longuet-Higgins [13] or Mei [15]):

$$\vec{f}_{20} \cdot \vec{i} = \frac{1}{2}|R_1|^2 \tag{C-2}$$

Using energy conservation and the Haskind-relations one obtains a relation between the first-order damping and exciting forces (Mei [15] or Newman [17]) which in the dimensionless quantities used in this work takes the form

$$b_{11} = K|\vec{f}_1 \cdot \vec{i}|^2 \ , \quad b_{22} = K|\vec{f}_1 \cdot \vec{j}|^2 \tag{C-3}$$

where $b_{11}$ and $b_{22}$ are the dimensionless damping force for sway and heave respectively. For the moment the same relation holds

$$b_{66} = K|M_1|^2 \tag{C-4}$$

where $b_{66}$ is the dimensionless damping moment.

In the solution of the radiation problem another useful check is the equation

$$Kb_{ii} = |A_i|^2 \ , \quad i=1,2,6 \tag{C-5}$$

Here $A_i$ is the amplitude of the radiated wave and the equation states that the energy flux away from the cylinder must be balanced by the work done by the cylinder on the fluid.

REFERENCES

[1] Abramowitz & Stegun: "Handbook of mathematical functions". Dover Publications.

[2] Andersen, Poul & Wuzhou, He: "On the calculation of two-dimensional added mass and damping coefficients by simple Green's function technique". The Technical University of Denmark, Rep. No. 287, June 1984.

[3] Chaplin, John R.: "On the irrotational flow around a horizontal cylinder in waves". Journal of Appl.Mech., Vol. 48, 1981.

[4] Chaplin, John R.: "Mass transport around a horizontal cylinder beneath waves". Journal of Fluid Mechanics, Vol. 140, 1984.

[5] Chaplin, John R.: "Nonlinear forces on a horizontal cylinder beneath waves". Journal of Fluid Mechanics, Vol. 147, 1984

[6] Dean, W.R.: "On the reflection of surface waves by a submerged circular cylinder". Proc.Camb.Phil.Soc. 44, 1948.

[7] de Boor, Carl: "A practical guide to splines". Springer-Verlag.

[8] Evans, Jeffrey, Salter & Taylor: "Sumberged cylinder wave energy device: theory and experiment". Appl.Oc.Res., Vol. 1, No. 1, 1979.

[9] Grue, John & Palm, Enok: "Reflection of surface waves by submerged cylinders". Appl.Oc.Res., Vol. 6, No. 1, 1984.

[10] Grue, John & Palm, Enok: "Wave radiation and wave diffraction from a submerged body in a uniform current". Journal of Fluid Mechanics, Vol. 151, 1985.

[11] Leppington, F.G. & Siew, P.F.: "Scattering of surface waves by a submerged cylinder". Appl.Oc.Res., Vol. 2, No. 3, 1980.

[12] Levine, Harold: "Scattering of surface waves by a submerged circular cylinder". Journal of Mathematical Physics, Vol. 6, No. 8, 1965.

[13] Longuet-Higgins, M.S.: "The mean forces exerted by waves on floating and submerged bodies with applications to sand bars and wave power machines". Proc.Roy.Soc., London, A.352, 1977.

[14] Mehlum, Even: "A circular cylinder in water waves". Appl.Oc.Res., Vol. 2, 1980.

[15] Mei, Chiang C.: "The applied dynamics of ocean surface waves". John Wiley & Sons.

[16] Milne-Thomson, L.M.: "Theoretical hydrodynamics". (5th ed) Macmillan, London, 1968.

[17] Newman, J.N.: "Marine hydrodynamics". The MIT press.

[18] Ogilvie, T. Francis: "First- and second-order forces on a cylinder submerged under a free surface". Journal of Fluid Mechanics, Vol. 16, 1963.

[19] Potash, R.L.: "Second-order theory of oscillating cylinders" Journal of Ship Res., Dec. 1971.

[20] Schnute, Jon T.: "The scattering of surface waves by two submerged cylinders". Proc.Camb.Phil.Soc., Vol. 69, 1971.

[21] Ursell, F.: "Surface waves on deep water in the presence of a submerged circular cylinder". Proc.Camb.Phil.Soc., Vol. 49, 1950.

[22] Vinje, T., Brevig, P. & Greenhow, M.: "Extreme wave forces on submerged cylinders". 2nd int.symp. on waves and tidal energy, 1981.

[23] Wehausen, J.V. & Laitone, E.V.: "Surface Waves". Handbuch der Physik, Vol. 9, 1960.